Cancer Cell International

RESEARCH

Open Access

Darunavir analog precursors target mitochondrial metabolism in multiple myeloma and CLL.

Marisabel Mecca[1], Marzia Sichetti[1], Enrico La Spina[2], Martina Giuseffi[1], Eugenia Giglio[1], Simona Picerno[1], Luciana Valvano[1], Teodora Statuto[1], Alessandro Santarsiere[3], Maria Funicello[3], Maria Francesca Armentano[4], Lucia Chiummiento[3], Paolo Lupattelli[5], Alessandra Romano[6], Antonio Giordano[7,8] and Salvatore Cortellino[9,10,11*]

Abstract

Background Multiple myeloma (MM) and chronic lymphocytic leukemia (CLL) are hematological malignancies with poor prognosis due to drug resistance, with no effective therapies. Drug resistance occurs from alterations in microenvironment and metabolism. Impaired mitochondrial metabolism underlies drug resistance in MM and CLL, and drugs targeting mitochondrial respiration show cytotoxicity and increase chemotherapy sensitivity. HIV protease inhibitors like nelfinavir show antitumor activity and resensitize drug-resistant cells to bortezomib and venetoclax. We evaluated effects of two HIV protease inhibitor precursors, BupM-NH2 and BnpM-NH2, on MM and CLL cells and their mechanism.

Methods The cytotoxicity of the compounds was evaluated in MM (MM1S and RPMI-8226) and CLL (HG3) cell lines, peripheral blood mononuclear cells (PBMCs) and in patient-derived MM cells using MTS assays. Apoptosis was assessed by Annexin V staining and cell cycle analysis using flow cytometry. Western blotting was employed to assess protein expression to investigate the effects of the tested compounds on autophagy, endoplasmic reticulum stress, and respiratory chain function. Cellular metabolic activity was measured using Seahorse analyzer, whereas mitochondrial function and ROS generation were quantified via flow cytometry with MitoSOX and MitoTracker staining.

Results BupM-NH2 and BnpM-NH2 at 50 µM decreased MM and CLL cell viability by 60% and 90%, while reducing PBMC viability by 40% and 50%. These compounds inhibited autophagy and mitochondrial respiration, reducing ATP production by 70% in MM, 30–60% in CLL, and 50% in PBMCs. BnpM-NH2 decreased the viability of cells from newly diagnosed multiple myeloma (NDMM) patients by 60% but showed a non-significant 15% reduction in relapsed/refractory multiple myeloma (RRMM) patients, whereas BupM-NH2 had no significant impact. Both compounds induced stress in respiratory chain and mitochondria that may help resensitize drug-resistant MM and CLL.

Conclusions BupM-NH2, and particularly BnpM-NH2, showed enhanced cytotoxicity against MM, CLL, and NDMM cells compared to PBMCs by inducing apoptosis through autophagy and mitochondrial respiration inhibition. While

*Correspondence:
Salvatore Cortellino
sacortel@yahoo.com

Full list of author information is available at the end of the article

© The Author(s) 2025. **Open Access** This article is licensed under a Creative Commons Attribution-NonCommercial-NoDerivatives 4.0 International License, which permits any non-commercial use, sharing, distribution and reproduction in any medium or format, as long as you give appropriate credit to the original author(s) and the source, provide a link to the Creative Commons licence, and indicate if you modified the licensed material. You do not have permission under this licence to share adapted material derived from this article or parts of it. The images or other third party material in this article are included in the article's Creative Commons licence, unless indicated otherwise in a credit line to the material. If material is not included in the article's Creative Commons licence and your intended use is not permitted by statutory regulation or exceeds the permitted use, you will need to obtain permission directly from the copyright holder. To view a copy of this licence, visit http://creativecommons.org/licenses/by-nc-nd/4.0/.

the cytotoxic effect in RRMM is less pronounced and nonsignificant, BupM-NH2 and BnpM-NH2 induces stress in respiratory chain and mitochondria, which may re-sensitize resistant tumor cells to treatments. Therefore these compounds may hold promise as novel therapeutic agents for MM and CLL treatment.

Keywords Multiple myeloma, Chronic lymphatic leukemia, HIV protease inhibitor, Autophagy, Mitochondria

Introduction

Neoplastic transformations caused by the accumulation of mutations in oncogenes or tumor suppressors are accompanied by changes in cellular metabolism [1, 2]. This metabolic change guarantees the supply of nutrients necessary to support anabolic pathways and tumor growth.

Many tumor types exhibit the Warburg effect, which is a metabolic reprogramming process characterized by a shift towards anaerobic glycolysis [3]. This metabolic change restricts oxidative phosphorylation (OXPHOS) and enables the synthesis of nucleotides, fatty acids, and antioxidants through intermediate products of glycolysis via the pentose phosphate pathway [4].

Recent studies have revealed that reprogramming of tumor cell metabolism is influenced not only by mutated oncogenic pathways, but also by the origin of the tissue and the environment in which the tumor develops [5–7]. Some tumors exhibit a preference for OXPHOS over glycolysis, utilizing fatty acids as an energy source via beta oxidation, and fueling the tricarboxylic acid (TCA) cycle through the catabolism of amino acids. B-cell hematological malignancies such as MM and chronic lymphocytic leukemia (CLL) rely on fatty acid metabolism and OXPHOS [8–11].

B cells undergo significant changes in cellular metabolism upon activation, including an increase in glycolytic activity and TCA cycle, as well as mitochondrial respiration, to meet the energetic and biosynthetic demands required for their function [12]. Both MM and CLL exhibit high consumption of glutamine and greatly elevated OXPHOS activity compared to their pre-malignant counterparts [10, 13] (Fig. 1). Moreover, enhanced mitochondrial mass and OXPHOS play a significant role in the development of drug resistance in MM and CLL cells, ultimately accelerating the progression of hematological malignancies [14, 15]. Increased ATP production through OXPHOS confers resistance to therapies in tumor cells by: (1) enhancing drug efflux via ATP-binding cassette (ABC) transporters, (2) suppressing apoptosis through activation of survival pathways, such as mTOR, and (3) circumventing energy deficits in nutrient-deprived environments by activating stress response pathways, including autophagy, essential for generating building blocks for proliferation and repair [16, 17]. Autophagy alleviates the cytotoxic effects of proteasome inhibitors, such as Bortezomib and Carfilzomib, by suppressing the unfolded protein response pathway (UPR), which is responsible for inducing apoptosis in tumor cells. Hematologic malignancies, such as MM and CLL, show elevated production of immunoglobulin proteins, which activate the UPR. Proteasome inhibition with Bortezomib and Carfilzomib leads to immunoglobulin accumulation, creating stress within tumor cells that triggers UPR pathways to initiate apoptosis. However, autophagy activation in resistant tumor cells facilitates immunoglobulin degradation, counteracting proteotoxic stress induced by proteasome inhibitors and suppressing apoptosis [18, 19] (Fig. 1).

Relapse occurs in approximately 20% of MM patients [20] and in 5–10% of those with CLL [21]. In patients with MM or CLL who develop resistance to therapy, their prognosis is poor, and their life expectancy decreases to less than two years. However, inhibiting the mitochondrial respiratory chain has demonstrated cytotoxicity towards primary and drug-resistant MM and CLL cells and has rendered resistant tumor cells susceptible to therapies once again [22–27].

Therapies for MM patients include proteasome inhibitors such as bortezomib and thalidomide analogs, cytotoxic medications (melphalan, cyclophosphamide, and doxorubicin), steroids, and radiotherapy [28, 29]. In contrast, patients with CLL are typically treated with nucleoside analogs, such as fludarabine, and alkylating agents, including cyclophosphamide, chlorambucil, and bendamustine, in combination with monoclonal antibodies targeting CD20, such as rituximab or obinutuzumab [30].

HIV protease inhibitors have demonstrated antineoplastic properties in several types of tumors, including leukemia, lung cancer, breast cancer, glioblastoma, MM, melanoma, and ovarian cancer [31–36]. These inhibitors exert their antitumor effects through various mechanisms, such as downregulation of Protein kinase B (AKT)/Signal Transducer and Activator of Transcription **3** (STAT3)/Extracellular Regulated Kinase (ERK) signaling [37–39], alteration of glucose metabolism, induction of endoplasmic reticulum stress via unfolded protein response (UPR) induction [40, 41], and anti-angiogenesis in vitro and in vivo [42, 43].

In addition, protease inhibitors can sensitize cells that develop resistance to various therapies. Clinical studies have assessed the antitumor efficacy of protease inhibitors, such as nelfinavir, against MM and leukemic cells that are resistant to bortezomib, a proteasome inhibitor, or have developed multiple resistance to bortezomib, lenalidomide, and pomalidomide in patients with MM [40, 44, 45].

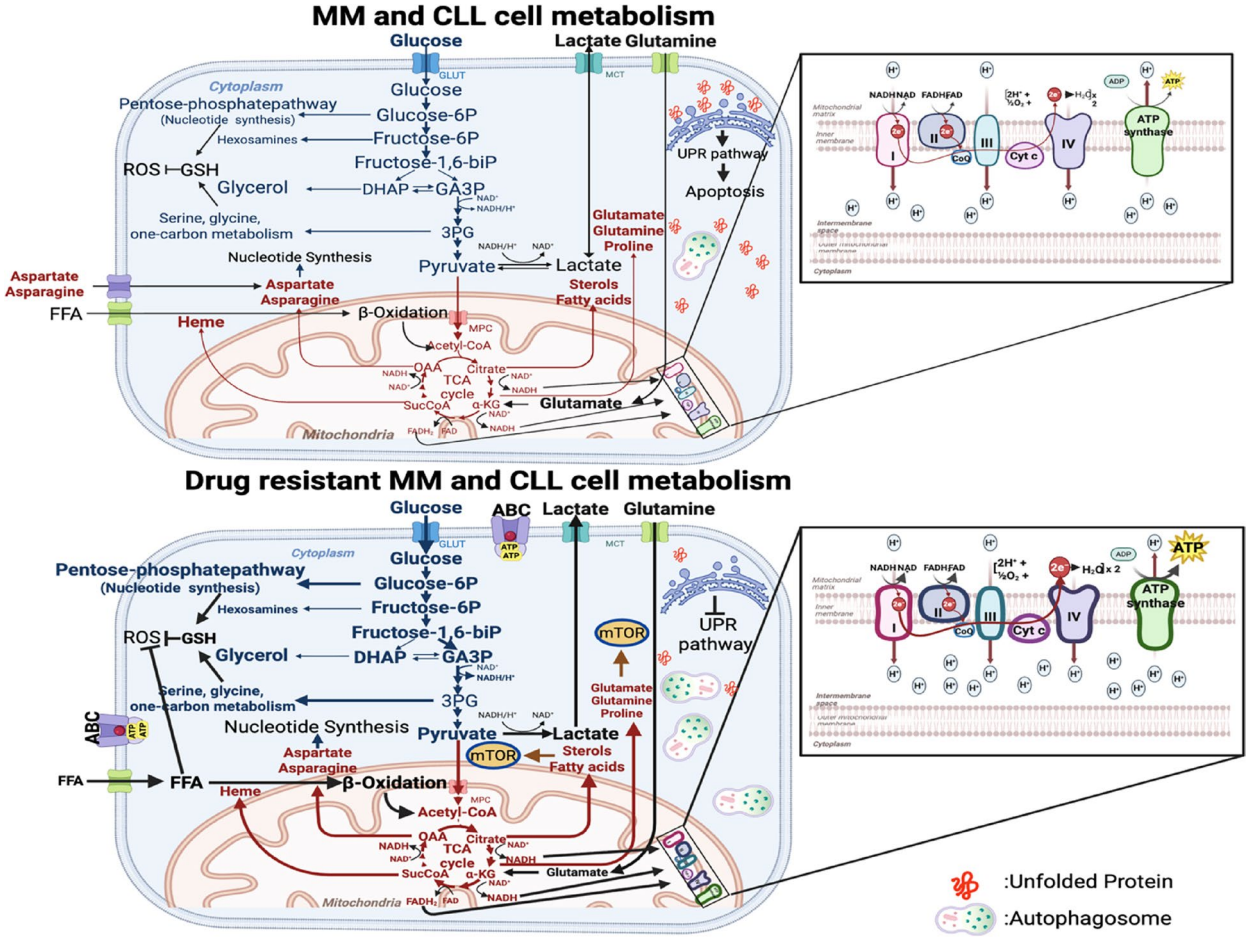

Fig. 1 Schematic representation of the metabolic changes occurring in therapy-resistant MM and CLL cells. The metabolism of therapy-sensitive myeloma cells primarily relies on aerobic glycolysis, with a partial dependence on oxidative phosphorylation. When myeloma cells develop resistance to therapy, they undergo metabolic reprogramming, resulting in increased mitochondrial mass and enhanced OXPHOS. This metabolic pathway comprises two components: the electron transport chain (ETC) and chemiosmosis. Within the ETC, electrons move through protein complexes, and the released energy is harnessed in chemiosmosis to produce ATP. The ETC contains four complexes, I through IV, which use electrons from NADH and $FADH_2$ to drive proton translocation, creating a proton gradient. This gradient is utilized by ATP synthase (Complex V) to catalyze ADP conversion to ATP. OXPHOS metabolism is mainly supported by heightened glycolysis, which generates pyruvate, and increased glutamine uptake, which fuels the Krebs cycle to produce alpha-ketoglutarate. Additionally, fatty acids undergo beta-oxidation to produce acetyl-CoA. Enhanced OXPHOS increases ATP production and Krebs cycle activity, supporting generation of intermediate metabolites essential for epigenetic reprogramming and lipid/cholesterol synthesis. High glucose uptake, metabolized through glycolysis is channeled into the pentose phosphate pathway, which supplies crucial intermediates necessary for the synthesis of nucleotides and glutathione (GSH). GSH is essential for maintaining REDOX balance and acts as an antioxidant to neutralize reactive oxygen species (ROS). These metabolic changes, which include increased synthesis of ATP, Krebs cycle intermediate metabolites, nucleotides and GSH, along with the activation of autophagy, strengthen and potentiate the pathways and mechanisms targeted by anticancer therapies, ultimately undermining their efficacy. ATP is crucial for the function of ATP-binding cassette (ABC) transporters, which expel chemotherapeutic agents from the cell, thereby reducing their intracellular concentration. The Krebs cycle facilitates the synthesis of glutamine via α-ketoglutarate (aKG) and the production of fatty acids and cholesterol via citrate, which can activate pro-tumor signaling pathways such as mTOR. Additionally, autophagy activation prevents immunoglobulin accumulation, which are naturally elevated in MM and CLL and increased by proteasome inhibitors. This reduction prevents apoptosis by mitigating the unfolded protein response (UPR) pathway. In the tumor microenvironment, drug-resistant tumor cells, under certain constrained conditions, maintain their mitochondrial metabolism by acquiring mitochondria from stromal and immune cells through nanotubes that establish intercellular connections (Created in https://BioRender.com)

Darunavir is an HIV protease inhibitor that has not demonstrated antitumor properties, unlike some of precursors of its analogues that have been found to be effective in inhibiting tumor progression. Previous research has shown that two compounds, RDD19 and RDD142, here named BupM-NH2 and BnpM-NH2, respectively, exhibit high toxicity in hepatocarcinoma cells (IC_{50} values of 57.05 and 67.96 μM) but are less toxic in hepatocytes (IC_{50} values greater than 150 μM). These compounds function by inhibiting proteasome activity and inducing apoptosis through the activation of the ER stress response pathway and autophagy [46].

In the present study, we examined the antitumor efficacy of these two compounds in MM and CLL tumor lines, as well as their cytotoxic effects on patient-derived bortezomib-lenalidomide-dexamethasone resistant MM cells.

Materials and methods

Key resources table

Reagent or resource	Source	Identifiers
Cell Lines and medium		
MM1S	ATCC	Cat#: CRL-2974; RRID: CVCL_8792
RPMI-8226	ATCC	Cat#: CCL-155; RRID: CVCL_0014
HG3	DSMZ	Cat#: ACC 765; RRID: CVCL_Y547
Cell culture medium and reagents		
RPMI-1640 Medium	Thermo Fisher Scientific (GIBCO)	Cat#: 11,875,093
Trypsin–EDTA Solution	Thermo Fisher Scientific	Cat#: R001100
Dulbecco's Phosphate Buffered Saline	Thermo Fisher Scientific	Cat#: 14,190,144
L–Glutamine	Thermo Fisher Scientific	Cat#: 25,030,081
Penicillin-Streptomycin Solution	Thermo Fisher Scientific	Cat#: 15,140,130
Fetal Bovine Serum	Thermo Fisher Scientific	Cat#: A3160502
Dulbecco's Phosphate Buffered Saline	Thermo Fisher Scientific	Cat#: 14,190,144
DMSO	Thermo Fisher Scientific	Cat#: 67–68-5
Lymphocyte Separation medium 1077	Sigma Aldrich-Merck	Cat#: C-44,010
Assay kit		
FITC annexin V-PI apoptosis detection kit I	BD Biosciences	Cat#: 556,547
MitoTracker Red CMXRos	Invitrogen	Cat#: M46752
MitoSOX Green Mitochondrial Superoxide Indicators	Invitrogen	Cat#: M36006
MTS AQueous CellTiter 96	Promega	Cat#: G111A
Primary Antibodies		
β-Actin (1:1000, 45 kDa)	Cell Signaling Technology	Cat#: 4967; RRID: AB_330288
ATF4 (1:1000, 45 KDa)	Proteintech	Cat#: 10835-1-AP; RRID: AB_2058600
ATP5A1 (1:10000, 55 KDa)	Proteintech	#14676-1-AP; RRID: AB_2061761
Beclin-1 (1:1000, 60 KDa)	Cell Signaling Technology	Cat#: 3738; RRID: AB_490837
Cleaved Caspase-3 (Asp175) (1:1000, 17/19 KDa)	Cell Signaling Technology	#9661; RRID: AB_2341188
Caspase-3 (1:1000, 17/19/35 KDa)	Cell Signaling Technology	Cat#: 9665; RRID: AB_2069872
Phospho-eIF2α (Ser51) (1:1000,65 KDa)	Cell Signaling Technology	Cat#: 3398; RRID: AB_2096481
EIF2a (1:1000, 65 kDa)	Abcam	Cat#: ab181467
LC3B (1:5000, 14/18 KDa)	Proteintech	Cat#: 14600-1-AP; RRID: AB_2137737
MTCO2 (1:6000, 26 KDa)	Proteintech	Cat#: 55070-1-AP; RRID: AB_10859832
NDUFB8 (1:10000, 22 KDa)	Proteintech	Cat#: 14794-1-AP; RRID: AB_2150970
p21 (1:2000, 21 KDa)	Proteintech	Cat#: 10355-1-AP; RRID: AB_2077682
p62 (1:10000, 62 KDa)	Proteintech	Cat#: 18420-1-AP; RRID: AB_10694431
SDHB (1:10000, 32 KDa)	Proteintech	Cat#: 10620-1-AP; RRID: AB_2285522
TOM20 (1:5000, 16 KDa)	Proteintech	Cat#: 11802-1-AP; RRID: AB_2207530
α-Tubulin (1:1000, 52 kDa)	Cell Signaling Technology	Cat#: 3873; RRID: AB_1904178
UQCRC2 (1:6000, 48 KDa)	Proteintech	Cat#: 14742-1-AP; RRID: AB_2241442
XBP-1s (1:1000, 60 KDa)	Cell Signaling Technology	Cat#: 12,782; RRID: AB_2687943
Secondary Antibodies		
Anti-mouse IgG HRP-linked (1:3000)	Cell Signaling Technology	Cat#: 7076; RRID: AB_330924
Anti-rabbit IgG HRP-linked (1:3000)	Cell Signaling Technology	Cat#: 7074; RRID: AB_2099233
WB Reagents		
Bio-Rad Protein Assay Dye Reagent Concentrate	Bio-Rad Laboratories	Cat#: 500-0006
Clarity Western ECL Substrate	Bio-Rad Laboratories	Cat#: 170–5061
Halt Phosphatase Inhibitor Cocktail	Thermo Fisher Scientific	Cat#: 1,861,277
Halt Protease Inhibitor Cocktail	Thermo Fisher Scientific	Cat#: 1,862,209
Pierce RIPA buffer	Thermo Fisher Scientific	Cat#: 89,901
Seahorse kit and reagents		
Seahorse XF Real-Time ATP Rate Assay Kit	Agilent Technologies	Cat#: 103592-100
Seahorse XF Cell Mito Stress Test Kit	Agilent Technologies	Cat#: 103015-100
Seahorse XFe96/XF Pro PDL Cell Culture Microplates	Agilent Technologies	Cat#: 103799-100
Seahorse XF RPMI medium	Agilent Technologies	Cat#: 103576-100
Seahorse XF 1.0 M glucose solution	Agilent Technologies	Cat#: 103577-100
Seahorse XF 100 mM pyruvate solution	Agilent Technologies	Cat#: 103578-100
Seahorse XF 200 mM glutamine solution	Agilent Technologies	Cat#: 103579-100
Rotenone	Sigma Aldrich-Merck	Cat#: R8875
$CD138^{+}$human cells isolation		
AutoMACS ProSeparator	MiltenyiBiotec	Cat#:130-092-545
StraightFrom Whole Blood CD138 MicroBeads	MiltenyiBiotec	Cat#:130-093-062

Chemicals

(2*R*,3*S*) *N*-(3-Amino-2-hydroxy-4-phenyl-butyl)-*N*-isobutyl-4-methoxy-benzenesulfonamide (BupM-NH2 alias RDD19) and (2*R*,3*S*) *N*-(3-Amino-2-hydroxy-4-phenyl-butyl)-*N*-benzyl-4-methoxy-benzenesulfonamide (BnpM-NH2 alias RDD142) were synthesized, purified, and finally characterized by NMR, according to the previously reported general procedure [46, 47].

Cell cultures and culture conditions

MM1S, RPMI-8226, and HG3 cells were cultured in complete RPMI 1640 medium supplemented with 10% heat-inactivated fetal bovine serum (FBS), 100 U/mL penicillin, 100 mg/mL streptomycin, and 2 mM of glutamine.

PBMCs were isolated from healthy ($n = 5$) heparinized blood by density gradient centrifugation over Lymphocyte Separation Medium 1077, according to manufacturer's instructions, and were used as non-pathological cells.

PBMCs were washed twice with sterile PBS and cell viability was assessed by the trypan blue exclusion assay. PBMCs were cultured at density of 1×10^6 cells/ml in complete RPMI 1640 medium. All cells were cultured at 37 °C in humidified atmosphere containing 5% CO_2 humidified atmosphere and cell cultures were routinely screened for mycoplasma contamination.

All the compounds were solubilized in DMSO as 100 mM stock solutions and stored at − 20 °C until use. The working solutions were freshly prepared and diluted in cell culture medium. The final concentration of DMSO was always within the limit of 0.8% (v/v), which did not affect cell growth.

Experiments were carried out at 70% cell confluence and performed in at least three independent biological replicates.

Isolation of CD138$^+$ cells from patient samples

All human samples used in this study were obtained from participants enrolled in a clinical study (n.34/2019/PO), which was approved by the independent Ethics Committee of Policlinico Catania 1. All procedures adhered to the ethical standards of the responsible committee on human experimentation, both institutional and national, and conformed to the Helsinki Declaration of 1975, as revised in 2024. Informed consent for data processing was obtained from all participants.

CD138$^+$ MM cells were isolated from patient samples using the Miltenyi MACSQuant Separator, according to the manufacturer's protocol. Briefly, 2 mL of bone marrow samples from patients were collected in 15 mL tubes and magnetically labeled with StraightFrom Whole Blood CD138 MicroBeads (MiltenyiBiotec). The "posselwb" program was utilized for the separation of CD138$^+$ cells on the autoMACS Pro Separator (Miltenyi Biotec). The purity of the isolated CD138$^+$ cells was evaluated by flow cytometry.

Multiple myeloma cells were isolated from three patients at the onset of the disease (NDMM) and five patients exhibiting resistance to bortezomib, lenalidomide, and dexamethasone (RRMM). These cells served as biological replicates to evaluate the impact of BupM-NH2 and BnpM-NH2 on apoptosis and mitochondrial ROS production. For each experimental setup, we conducted technical triplicates for each patient cell line under all experimental conditions.

Observation of morphological changes

MM1S, RPMI-8226 and HG3 cells were seeded into 24-well plates (1.5×10^5 cells per well) and cultured overnight, while PBMCs were seeded at concentration of 1×10^6 cells/ml per well. They were treated for 24 h, 48 h and 72 h with different concentrations of BupM-NH2 and BnpM-NH2 (10 μM, 30 μM, 50 μM), using untreated cells and cells treated with DMSO as negative controls. Cellular morphology was observed at inverted optical microscope (Axio Vert A1, Zeiss).

Cell viability assay

Cell viability under synthetic molecules treatment was analyzed by an MTS assay: 3×10^4 cancer cells and 1×10^5 PBMCs were plated in 96-well plates in 100 μL of standard medium and incubated at 37 °C and 5% CO_2. The day after 50 μL of medium supplemented with different concentrations of BupM-NH2 and BnpM-NH2 (10 μM, 30 μM, 50 μM) were added to the wells. As a negative control, cells were treated with DMSO at the highest concentration used in the treatments. 24 h, 48 h and 72 h after treatment, 20 μL of MTS AQueous CellTiter 96 was added to the culture media and after 2 h of incubation at 37 °C the absorbance at 490 nm with a reference wavelength of 550 nm was recorded by using VICTOR Nivo Multimode Microplate Reader (PerkinElmer, Life and Analytical Sciences). The quantity of formazan produced, as measured by absorbance at 490 nm, is directly proportional to the number of living cells in culture. The viability of cells treated with increasing concentrations of drugs was tested relative to the viability of the same cells treated with DMSO and IC_{50} values.

IC50 values were determined by plotting inhibitor concentration logarithm on the x-axis against normalized response on the y-axis, followed by nonlinear regression (log(inhibitor) vs. normalized response-Variable slope) using GraphPad Prism 10 statistics software (GraphPad, La Jolla, CA, USA). The normalized response was calculated by converting MTS absorbance to inhibition percentage, ranging from 0% (signal from untreated control without inhibitor) to 100% (maximum inhibition). The

equation for this model is: Y = 100/(1 + 10^(X-LogIC50)). Experiments were performed in triplicates.

Western blotting analysis

MM1S, RPMI-8226 and HG3 cells were seeded in a 100 mm dish at 2.5×10^6 cells per dish and treated for 48 h at the concentrations of 10 μM, 30 μM, and 50 μM of BupM-NH2 and BnpM-NH2; then they were collected and lysed for 30 min in ice-cold Pierce RIPA buffer, supplemented with a mixture of 1% Phosphatase Inhibitor Cocktail and 1% Protease Inhibitor Cocktail. All the samples were also sonicated for 30 min at 37% power with the BANDELIN Sonorex DT sonicator (Bandelin, Berlin, Germany) and then centrifuged at 13,000 rpm for 10 min at 4 °C to remove insoluble cell debris.

Protein content was quantified using the Bio-Rad Protein Assay Dye Reagent, based on the Bradford method. Aliquots, containing 30 μg of proteins from each lysate cell, were separated by SDS polyacrylamide gel electrophoresis and transferred to a polyvinylidene difluoride membrane using a Trans Blot Turbo Transfer System.

The membranes (Bio-Rad Laboratories, Hercules, CA, USA) were blocked for 1 h at room temperature with 5% nonfat milk in TPBS (PBS with 0.1% Tween 20) and then probed overnight with the primary antibodies.

The membranes were then washed three times with wash buffer (TPBS), incubated with a corresponding horseradish peroxidase-conjugated secondary antibody, and the signals were developed using the enhanced chemiluminescence kit (Clarity™ Western ECL Substrate, Bio-RadLaboratories Inc.). The chemiluminescent signal was detected by using the chemiluminescence system ChemiDoc Imaging System XRS+ (Bio-Rad, Hercules, California, USA) with the ImageLab software and quantified by densitometric analysis of the bands using the ImageJ Lab 4.1 software (Bio-Rad, Hercules, California, USA) on independent replicates.

FACS analysis

1.Cell cycle analysis and apoptosis assay

Cell cycle determination and apoptosis analysis were performed as described below. 5×10^5 MM1S, RPMI-8226 and HG3 cells and 3×10^6 PBMCs were seeded in a six-well plate and treated with 30 μM BupM-NH2 and BnpM-NH2. Cells treated with DMSO represented negative controls.

After 48 h of treatment, cells were harvested, washed twice with cold PBS, and resuspended in Binding Buffer at a concentration of 1×10^6 cells/ml (FITC Annexin V Apoptosis Detection Kit I, BD Pharmigen, Franklin Lakes, NJ, USA). Then, 100 μL of the cell suspensions were mixed with 5 μL of Annexin V-FITC and 5 μL of propidium iodide (PI) and incubated for 15 min at room temperature in the dark. Then, 400 μL of Binding Buffer was added to each tube and the analysis was carried out by flow cytometry instrument FACS (Navios, Beckman Coulter, IN, USA) with the Kaluza 2.1 analysis software (Beckman Coulter). A total of 10^4 events for each sample were acquired and analyzed, obtaining the detection of live, early apoptotic, apoptotic, and necrotic cells.

The remaining cells were fixed in 70% ethanol, for at least 2 h at 4 °C, and stained with 50 μg/ml PI containing 10 μg/ml RNase A for 30 min at room temperature. Fluorescence cell analysis was performed with by using FACS (Navios, Beckman Coulter, IN, USA) and cell cycle distribution was analyzed in the form of percentage of cells in the G0/G1, S, and G2/M phases by Kaluza 2.1 analysis software (Beckman Coulter).

Three independent experiments were carried out for each assay.

2.Mitochondrial Analysis

MM1S, RPMI-8226 and HG3 mitochondrial mass and mitochondrial ROS levels under BupM-NH2 and BnpM-NH2 treatment were analyzed.

MitoTracker Red, a red-fluorescent mitochondrial stain which appears to localize to mitochondria regardless of mitochondrial membrane potential, was used to examine changes in mitochondrial mass following the manufacturer's instructions. Instead, MitoSOX Green mitochondrial superoxide indicator, a novel green-fluorogenic dye specifically targeted to mitochondria in live cells, was used to detect mitochondrial ROS, especially superoxide, following the manufacturer's instructions [48].

Briefly, MM1S, RPMI-8226 and HG3 cells were seeded in a 6-well plates at a density of 5×10^5 cells per well, and after 24 h were treated with 30 μM BupM-NH2 and BnpM-NH2. As a positive control, cells were treated with 5 μM rotenone. Cells treated with DMSO represented negative controls. The day after, the medium was removed and prewarmed (37 °C) staining solution containing 500 nM MitoTracker probe and 1 μM MitoSOX probe was added. After 30 min of incubation at 37 °C in the dark, cells were washed with PBS and analyzed by FACS (Navios, Beckman Coulter, IN, USA) with the Kaluza 2.1 analysis software (Beckman Coulter) [49]. MitoSOX Green has excitation and emission peaks at 488 and 510 nm, respectively, whereas MitoTracker Red has excitation and emission peaks at 579 and 599 nm, respectively.

Metabolic profiling by seahorse assays

Oxygen consumption rate (OCR) and extracellular acidification rate (ECAR) of MM1S, RPMI-8226, HG3 and PBMCs under 30 μM BupM-NH2 and BnpM-NH2 treatments conditions were measured with the Seahorse Extracellular Flux XF Pro Analyzer (Agilent, Santa Clara, CA, USA). Seahorse XF Real-Time ATP Rate Assay Kit and Seahorse XF Cell Mito Stress Test Kit protocols

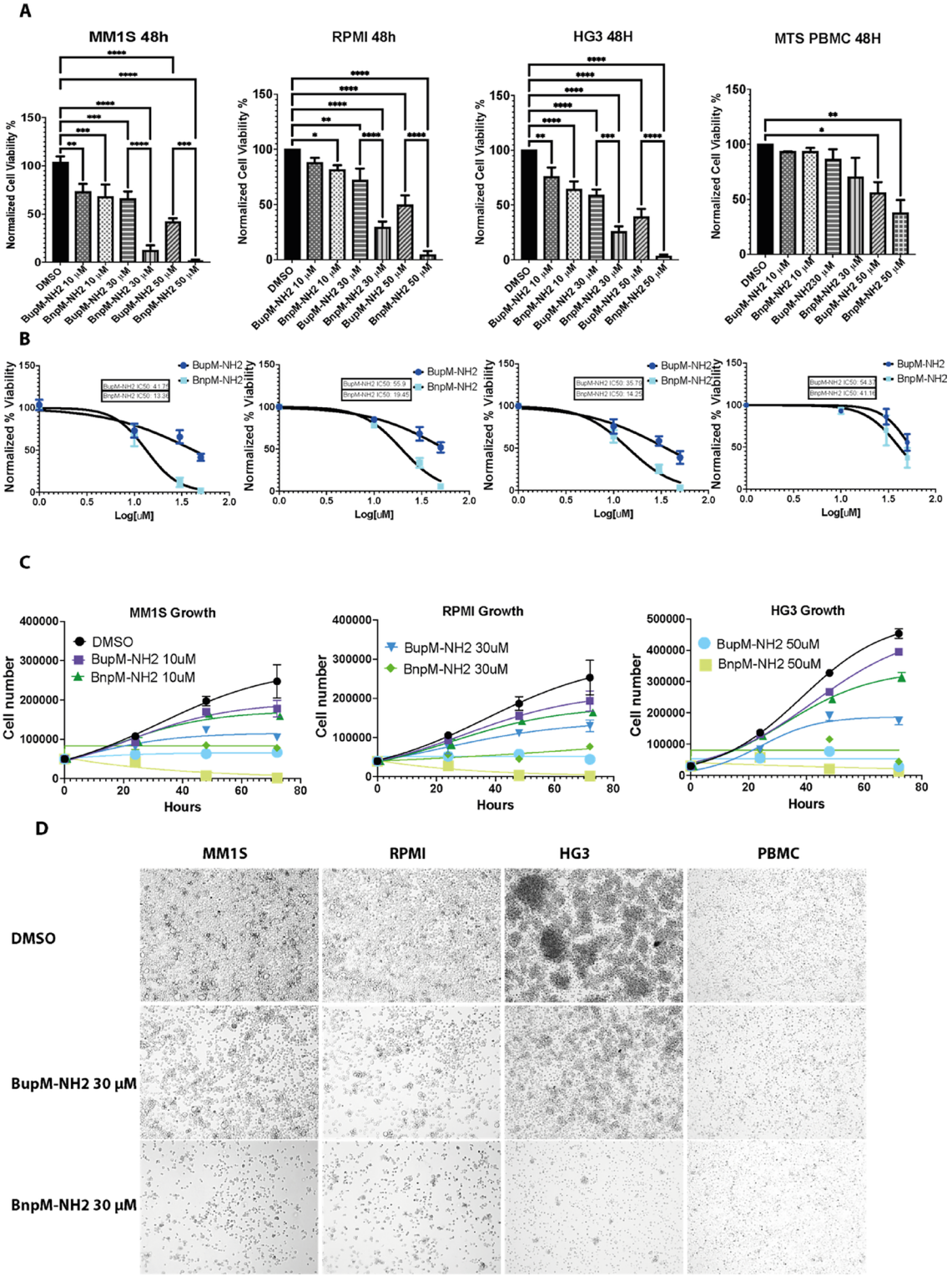

Fig. 2 (See legend on next page.)

(Agilent) were performed with the XF Pro analyzer, according to the manufacturer's instructions. Briefly 5×10^5 MM1S, RPMI-8226 and HG3 cells and 3×10^6 PBMCs were seeded in a six-well plate and treated with 30 µM BupM-NH2 and BnpM-NH2 and cultured for 24 h. Cells treated with DMSO function as negative controls, enabling the detection of effects on basal metabolism mediated by the vehicle in which BupM-NH2 and

(See figure on previous page.)

Fig. 2 Cytotoxicity of protease inhibitors BupM-NH2 and BnpM-NH2 in MM and leukemia cell lines. Cell viability assays (MTS) were performed with MM cell lines (MM1S, RPMI-8226), chronic lymphocytic leukemia cell line (HG3), and primary human PBMCs (**A**) and dose–response curves were obtained to calculate the IC_{50} values for the drugs in all cell lines (**B**). Cells were treated with increasing concentrations (10, 30 and 50μM) of BupM-NH2 and BnpM-NH2 for 48 h. Data represent the mean ± SD of at least three replicates. (**C**) Effect of BupM-NH2 and BnpM-NH2 on proliferation of MM1S, RPMI-8226 and HG3 was determined by counting viable cells. The cells were seeded and exposed to BupM-NH2 and BnpM-NH2 (10, 30 and 50μM) for 24, 48 and 72 h then collected and counted. DMSO treated cells served as control. The cells number was plotted against time to determine the cell growth curve. All assays were repeated in three independent experiments. (**D**) Light microscopy images showing the morphology of the cells after treatment with BupM-NH2 and BnpM-NH2 (30 μM) for 48 h. Statistical analysis was performed using one-way analysis of variance (ANOVA). P values were determined by one-way ANOVA with Tukey's post analysis Differences were considered significant when $P \leq 0.05$. All data are represented as mean ± SEM

BnpM-NH2 are dissolved. This facilitates the differentiation and precise determination of the activity of BupM-NH2 and BnpM-NH2 on glycolysis and OXPHOS in the analyzed cells. The next day cells were harvested, washed twice with cold XF-RPMI, and resuspended in XF RPMI medium supplemented with 1 mM pyruvate, 2 mM glutamine, 10 mM glucose according to the protocols. Then cells were counted and seeded in Seahorse XF PDL coated plates at a density of 3×10^4 per well for cancer cells and 2×10^5 for PBMCs. Cell cultures were allowed to equilibrate for 1 h at 37 °C in a no-CO_2 incubator and Seahorse XF Pro analysis was performed at 37 °C simultaneously measuring OCR (pmole O_2/min) and ECAR (mpH/min). All the parameters were normalized on cell number.

XF ATP Rate Assay measures OXPHOS and glycolysis's contribution to ATP production. OCR and ECAR were measured before and after sequential injection of 1.5 μM oligomycin and 0.5 μM rotenone/antimycin A.

XF Cell Mitochondrial Stress assay was performed to assess coupling of respiratory chain, maximal and non-mitochondrial oxygen consumption. OCR was analyzed under basal condition and after the injection into each well sequentially of 1.5 μM oligomycin, 1.5 μM carbonylcyanide-4(trifluoromethoxy)phenylhydrazone (FCCP), and a mixture 0.5 μM rotenone/antimycin A. The response to the minimal dose of oligomycin and FCCP, generating the maximal effect, accounts for non-phosphorylating mitochondrial respiration and maximal FCCP-uncoupled respiration, respectively. The response to the rotenone and antimycin A mixture accounts for non-mitochondrial oxygen consumption. Data were obtained from three independent experiments, where each sample was performed with at least 8 technical replicates. All data were assessed with XF Wave Software (Seahorse Bioscience, Agilent).

Statistical analysis

Statistical analysis was performed using GraphPad Prism (GraphPad Software, Inc., San Diego, CA, USA). Data were reported as mean ± standard deviation (SD) of, at least, three independent experiments performed in triplicate and were compared by an unpaired Student's t-test or ANOVA for multiple comparisons. For both One-Way ANOVA and Two-Way ANOVA, Tukey's post-hoc multiple comparisons were applied as recommended by Prism. According to the *p*-value, differences were considered statistically significant when the value of $^*P < 0.05$.

Results

The compounds BupM-NH2 and BnpM-NH2 inhibit the proliferation of MM (MM1S and RPMI-8226) and CLL (HG3) cell lines

We conducted a 48-hour MTS assay to evaluate the impact of compounds BupM-NH2 and BnpM-NH2 on the viability of human MM and CLL cell lines and PBMCs obtained from healthy subjects. Both compounds significantly reduced the viability of MM1S and RPMI-8226 MM cells, as well as HG3 CLLs, in a dose-dependent manner (30 and 50 μM), although their effect on PBMCs was milder (Fig. 2A). BnpM-NH2 is more effective, with IC_{50} values of 13.36, 19.45, and 14.25 μM in MM1S, RPMI-8226, and HG3, respectively, while BupM-NH2 had higher IC_{50} values in all three cell lines: 41.75, 55.9, and 35.79 μM in MM1S, RPMI-8226, and HG3, respectively. The toxicity of BupM-NH2 and BnpM-NH2 compounds was reduced in PBMCs, with IC_{50} values of 54.37 and 41.16 μM, respectively (Fig. 2B).

To determine whether the compounds exhibited cytostatic or cytotoxic properties, we conducted a 72-hour growth curve experiment. While BupM-NH2 exhibited a cytostatic effect at both concentrations, BnpM-NH_2 inhibited cell growth at 30 μM and was cytotoxic at 50 μM (Fig. 2C-D).

Cell cycle analysis showed that both compounds at a concentration of 30 μM, halted tumor cells in the G1 phase, decreasing the number of cells in the S phase (in Supplementary Fig. 1 A). BnpM-NH_2 had the most significant effect on blocking tumor cells in the G1 phase, as it triggered the upregulation of p21, a mediator that promotes the arrest of cells in the G1 phase, particularly in MM1S and RPMI-8226 MM cells (Supplementary Fig. 1B).

Unlike the results observed in hepatocarcinoma cells [46], BnpM-NH_2 exhibited significantly greater antitumor effectiveness against MM and CLL cells than BupM-NH2, accompanied by lower toxicity in PBMCs.

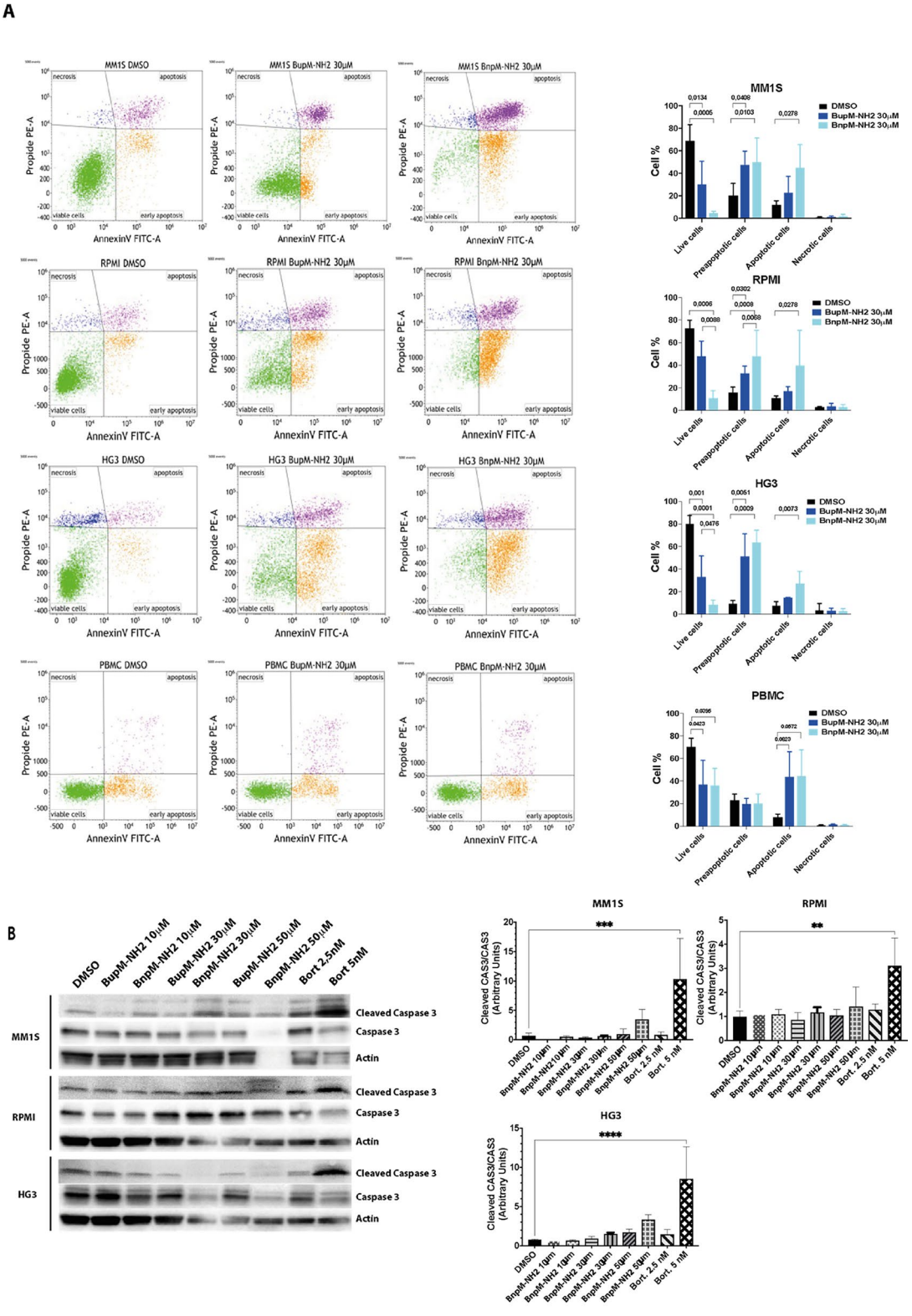

Fig. 3 (See legend on next page.)

(See figure on previous page.)

Fig. 3 Precursors of Darunavir analogues, BupM-NH2 and BnpM-NH2, induce apoptosis in MM and CLL cells independently of caspase-3 activation. (**A**) Apoptosis rates in MM (MM1S and RPMI-8226) and CLL (HG3) cells treated with BupM-NH2 and BnpM-NH2 (30μM) for 48 h were determined using Annexin V/FITC-PI flow cytometry. Representative flow cytometry images and bar graphs of apoptotic cell rates are shown. Average values per treatment were calculated from three independent experiments and presented as mean ± SD. (**B**) Expression of cleaved and total caspase 3 in MM and CLL cells, treated with BupM-NH2 and BnpM-NH2 (10,30 and 50 μM) and Bortezomib (2,5 and 5 nM) for 48 h, was analyzed by WB. The ratio of cleaved-caspase-3/caspase-3 intensities, normalized to actin, was statistically analyzed and represented as mean ± SD from three independent experiments in bar graph. P values were determined by one-way ANOVA with Tukey's post analysis Differences were considered significant when $P \leq 0.05$

BupM-NH2 and BnpM-NH2 induce apoptosis in MM and CLL cancer cells

We subsequently assessed whether the cytotoxicity of the compounds resulted from necrosis or apoptosis by performing an annexin V assay. Both compounds, at a concentration of 30μM, increased the proportion of MM and leukemia cells undergoing pre-apoptosis and apoptosis (Fig. 3A). Notably, BnpM-NH2 proved more effective in inducing apoptosis in all tumor cell lines, surpassing even Saquinavir (30μM), another HIV protease inhibitor known for its anti-tumoral activity (Supplementary Fig. 2 A).

BnpM-NH2 modestly increases cleaved caspase-3 expression at higher concentrations (30 and 50μM) after 48 h in MM1s (Δ0.313 ± 5.0, $p = 0.999$; Δ7.137 ± 5.0, $p = 0.776$) and HG3s (Δ1.085 ± 2.3, $p = 0.998$; Δ3.626 ± 2.3, $p = 0.711$), though difference was not statistically significance. This enhancement is less pronounced in RPMIs (Δ0.259 ± 0.44, $p = 0.998$; Δ0.654 ± 0.44, $p = 0.748$), where total caspase-3 expression increases (Fig. 3B). Nevertheless, BnpM-NH2 demonstrates reduced efficacy in cleaved caspase-3 activation compared with bortezomib. These disparities may be attributed to the distinct mechanisms of action of each compound.

BupM-NH2 and BnpM-NH2 suppress UPR pathway and autophagic flux

Since several HIV protease inhibitors exert their antitumor effects by inducing endoplasmic reticulum (ER) stress and ultimately triggering UPR-mediated apoptosis [50, 51] we evaluated the effect of BupM-NH2 and BnpM-NH2 on the expression and activation of key components of the UPR pathway, including activating transcription factor 4 (ATF4), the spliced form of X-box binding protein 1 (XBP1s), as well as the phosphorylation of eukaryotic translation initiation factor 2 alpha (eIF2α). Unexpectedly, control cells treated with DMSO showed higher ATF4 and XBP1s expression than cells treated with BupM-NH2 and BnpM-NH2 (30 μM) for 48 h. Compared to DMSO controls, BupM-NH2 and BnpM-NH2 significantly reduced ATF4 expression in three cell lines: MM1S (Δ0.563 ± 0.08, $p = 0.0015$; Δ0.578 ± 0.08, $p = 0.0013$), RPMI (Δ0.683 ± 0.12, $p = 0.0043$; Δ0.719 ± 0.12, $p = 0.0033$), and HG3 (Δ0.783 ± 0.045, $p = 0.0001$; Δ0.891 ± 0.045, $p = 0.0001$). Treatment also decreased XBP1s levels in MM1S (Δ0.522 ± 0.12, $p = 0.0157$; Δ0.408 ± 0.12, $p = 0.0442$), RPMI (Δ0.425 ± 0.08, $p = 0.0047$; Δ0.396 ± 0.08, $p = 0.0066$), and HG3 (Δ0.492 ± 0.06, $p = 0.0009$; Δ0.369 ± 0.06, $p = 0.0040$) (Fig. 4A). The elevated levels of UPR stress markers in DMSO treated cells may be due to intrinsically high protein turnover and unfolded protein stress in these tumor cells expressing elevated immunoglobulin. Nevertheless, the upregulation of the UPR signaling pathway was independent of DMSO treatment, as this pathway remained upregulated in untreated cells (Supplementary Fig. 2B). Moreover, treatment with saquinavir affected autophagy differently than the compounds we tested, as it triggered the expression of ATF4 and the phosphorylation of eIF2α, both of which indicate the activation of the UPR pathway (Supplementary Fig. 2 C).

HIV protease inhibitors also regulate autophagy and proteasomal activities [40, 41, 52, 53]. Previous studies have shown that BupM-NH2 and BnpM-NH2 activate autophagy and inhibit the proteasome, resulting in the accumulation of ubiquitinated proteins and ER stress-induced apoptosis [46]. However, in hematological tumors, BupM-NH2 and BnpM-NH2 affect autophagy differently, as they increase the lipidated form of microtubule-associated protein light chain 3 (LC3B) and the expression of P62, which is degraded via autophagy. In comparison to DMSO-treated control cells, BupM-NH2 and BnpM-NH2 significantly elevated LC3B expression as follows: (Δ1.780 ± 0.055, $p < 0.0001$; Δ2.939 ± 0.055, $p < 0.0001$) in MM1S; (Δ0.824 ± 0.40, $p = 0.1873$; Δ3.166 ± 0.040, $p < 0.0006$) in RPMI; (Δ2.254 ± 0.75, $p = 0.0557$; Δ4.277 ± 0.075, $p < 0.0032$) in HG3. Additionally, BupM-NH2 and BnpM-NH2 increased p62 levels as follows: (Δ2.439 ± 0.70, $p = 0.0317$; Δ2.549 ± 0.70, $p < 0.0264$) in MM1S; (Δ0.891 ± 0.35, $p = 0.1001$; Δ1.504 ± 0.35, $p < 0.0128$) in RPMI; (Δ0.891 ± 0.25, $p = 0.0303$; Δ0.996 ± 0.25, $p < 0.0189$). The expression of Beclin1 (BECN1), a marker of autophagy activation, remained unchanged in samples treated with BupM-NH2, whereas it increased in MM1S and RPMI-8226 treated with BnpM-NH2 (Fig. 4B). The increase in lipidated LC3B and P62 suggests that autophagic flux (the fusion of autophagosome with lysosome) was blocked by treatment with BupM-NH2 and BnpM-NH2. Preliminary data further indicated that BupM-NH2 and BnpM-NH2 activate the mTOR pathway. The upregulation of mTOR is linked to the suppression of autophagy. This effect may represent a response to the alterations in autophagy or mitochondrial metabolism induced by BupM-NH2 and BnpM-NH2 (Supplementary

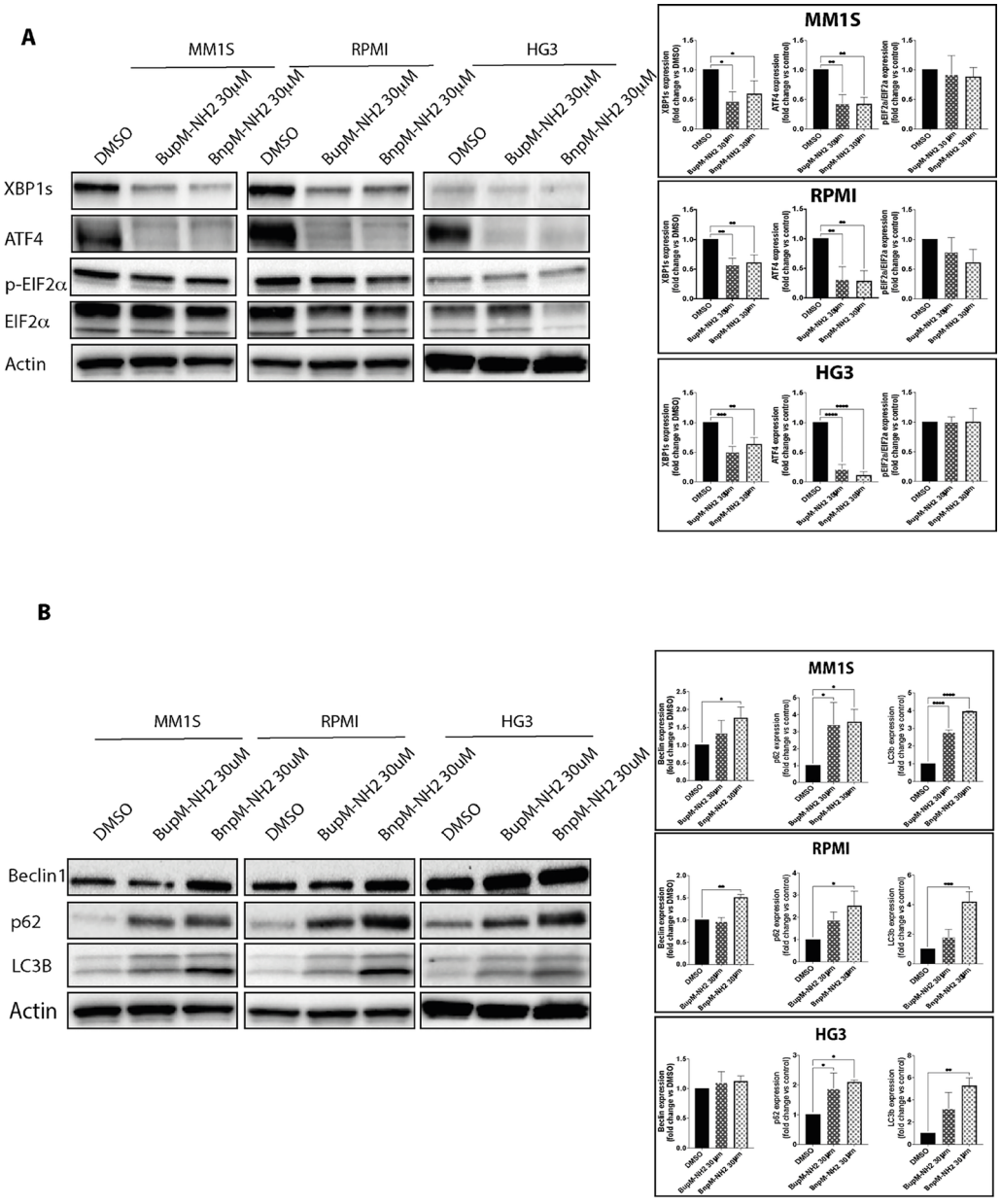

Fig. 4 BupM-NH2 and BnpM-NH2 inhibit autophagy without activating the ER stress response. (**A**) WB analysis of XBP1s, ATF4, p-eIF2α, and eIF2α expression in MM1S, RPMI-8226, and HG3 cells treated with BupM-NH2 and BnpM-NH2 (30 μM) for 48 h was performed. The intensity of XBP1s and ATF4, and the ratio of p-EIF2α/eIF2α intensity normalized to actin were quantified and plotted as bar graphs. The results are presented as mean ± SD of at least three replicates. (**B**) Beclin1, p62, and LC3b expression in MM and CLL cells treated with BupM-NH2 and BnpM-NH2 (30 μM) for 48 h was analyzed by WB. The bar graph quantitatively represents autophagy proteins normalized to actin. Data are presented as mean ± SD from a minimum of three replicates. P values were determined by one-way ANOVA with Tukey's post analysis Differences were considered significant when $P \leq 0.05$

Fig. 3 A). Saquinavir, in contrast, enhances the expression of Beclin1 while exerting a modest influence on the expression of p62 and lipidated LC3, which may suggest an augmentation in autophagy (Supplementary Fig. 2 C).

Moreover, the reduction in ER stress, inhibition of autophagy, and mild activation of cleaved CAS-3 dependent apoptosis indicates that the cytotoxicity of BupM-NH2 and BnpM-NH2 is mediated by alternative mechanisms.

BupM-NH2 and BnpM-NH2 trigger apoptosis in MM and leukemia cells by decreasing the activity of the mitochondrial respiratory system

Mitochondria are vital components of cellular energy metabolism and the regulation of apoptosis, and they play a key role in activating the integrated cytosolic response to stress and promoting cell survival and fitness. As nelfinavir, an HIV protease inhibitor, has been shown to induce caspase-independent cell death and

cell cycle arrest by disrupting respiratory chain function and increasing free radical production [54], we sought to determine whether BupM-NH2 and BnpM-NH2 could also act by impairing the respiratory chain.

Analysis of mitochondrial respiration performed by Seahorse revealed that cells treated with BupM-NH2 and BnpM-NH2 exhibited a reduced OCR (Δ69.38 ± 2.09 $p < 0{,}0001$; Δ72.19 ± 2.09, $p < 0{,}0001$ MM1S; Δ97.07 ± 3.89 $p < 0{,}0001$; Δ83.44 ± 3.89, $p < 0{,}0001$ RPMI; Δ15.36 ± 1.97 $p < 0{,}0001$; Δ37.17 ± 1.97, $p < 0{,}0001$ HG3; Δ33.56 ± 2.15 $p < 0{,}0001$; Δ33.12 ± 2.40, $p < 0{,}0001$ PBMC) compared to untreated cells, whereas ECAR was higher in treated cells than in untreated cells (Δ28,56 ± 1.65 $p < 0{,}0001$; Δ12,43 ± 1.65, $p < 0{,}0001$ MM1S; Δ28,96 ± 1.61 $p < 0{,}0001$; Δ27,10 ± 1.61, $p < 0{,}0001$ RPMI; Δ8.196 ± 1.14 $p < 0{,}0001$; Δ2.305 ± 1.14, $p = 0{,}1465$ HG3; Δ4.11 ± 2.15 $p < 0{,}0005$; Δ1.72 ± 2.40, $p = 0{,}1561$ PBMC) (Fig. 5). MM cells possess a higher OCR than CLL cells, indicating that their energy metabolism relies heavily on OXPHOS. Following a decrease in mitochondrial respiration, MM cells activated a compensatory mechanism by increasing ATP production via glycolysis. However, this increase in glycolysis did not occur in BnpM-NH_2 -treated HG3 cells. PBMCs exhibit OXPHOS-dependent metabolism. Although treatment with BupM-NH2 and BnpM-NH2 reduced ATP production via OXPHOS by approximately half, this effect was less pronounced than that observed in MM and CLL cell lines, where ATP production via OXPHOS was reduced by approximately 3–4 times (Fig. 5).

To assess the effects of these compounds on the mitochondrial ability to respond to stress or increased energy demands, we utilized the MitoStress Test on Seahorse to measure spare respiratory capacity (SRC). The results showed that treatment with BupM-NH2 and BnpM-NH2 led to a significant reduction in maximal mitochondrial respiration and impaired SRC (Supplementary Fig. 4), rendering cells unable to meet their energy requirements.

Subsequently, we sought to establish whether the modifications in mitochondrial metabolism caused by BupM-NH2 and BnpM-NH2 were associated with dysfunction of various respiratory chain complexes. To this end, we assessed the expression levels of specific subunits within each complex of the electron transport chain (ETC). Our investigation focused on the NADH dehydrogenase [ubiquinone] 1 beta subcomplex subunit 8 (NDUFB8) associated with complex I, the succinate dehydrogenase [ubiquinone] iron-sulfur subunit (SDHB) of complex II, the cytochrome b-c1 complex subunit 2 (UQCRC2) of complex III, the cytochrome c oxidase subunit 2 (MTCO2) of complex IV, and the ATP synthase F1 alpha subunit (ATP5F1A) of complex V. We found that BupM-NH2 and BnpM-NH2 decreased the expression of MTCO2 in complex IV of MM cells (Fig. 6A), whereas BnpM-NH_2 inhibited the expression of SDHB in complex II, particularly in leukemia cells, but also slightly in MM cells (Fig. 6A). These changes in mitochondrial metabolism were linked to an increase in both the expression and phosphorylation of AMPK, an energy sensor (Supplementary Fig. 3 A). However, treatment with saquinavir did not affect the expression of MTCO2, confirming that its mechanism of action differs from that of BupM-NH2 and BnpM-NH2 (Supplementary Fig. 2D), even though it impacts mitochondrial energy metabolism and induces both the expression and activation of AMPK (Supplementary Fig. 3B).

To assess the potential association between respiratory chain defects and alterations in ROS generation, Mitosox was used to quantify mitochondrial superoxide anion production by measuring changes in the fluorescence intensity distribution (% of Max) and mean fluorescence intensity (MFI) across the cell population. The median MFI signal in the treated population was compared with that of the DMSO-treated control to quantify the signal change through fold-change analysis. % of max was used to qualitatively detect changes in Mitosox signaling distribution between treated and control cell populations. Analyses showed that neither BupM-NH2 nor BnpM-NH2 significantly influenced superoxide anion production after 24 h of treatment, with no shift in signal distribution (% of Max) or intensity (MFI fold change) between the treated and control populations (Fig. 6B). Treatment of MM1S and RPMI-8226 cells with BupM-NH2 or BnpM-NH2 did not affect superoxide anion production after 24 h (Fig. 6B), with no variation in the percentage of Max or MFI fold changes. BnpM-NH2 slightly increased free radical production in HG3 leukemic cells, although the difference was not statistically significant, as shown by the %of Max histogram and MitoSox MFI ratio bar graph compared to the DMSO control. Rotenone, an ETC complex I inhibitor used as a control, significantly reduced ROS production in MM1S cells, but not in RPMI-8226 cells, and slightly increased superoxide anion production in HG3 cells, although not significantly, as shown in the MFI fold change bar graph. This aligns with literature reporting that rotenone can either increase or inhibit ROS production, depending on the cell line (Fig. 6B).

Mitochondrial mass analysis using MitoTracker suggested that BnpM-NH2 might increase mitochondrial mass, although this increase was not statistically significant. BnpM-NH2 induced a not statistically significant ($p > 0.05$) increase in the MitoTracker MFI in MM1S, RPMI-8226, and HG3 cells, with a negligible increase in MM1S cells (Fig. 6B). Rotenone increased MitoTracker fluorescence in HG3 cells, as shown by the curve shift and MFI fold-change but had no effect on MM1S and RPMI-8226 cells. BupM-NH2 induced a marginal,

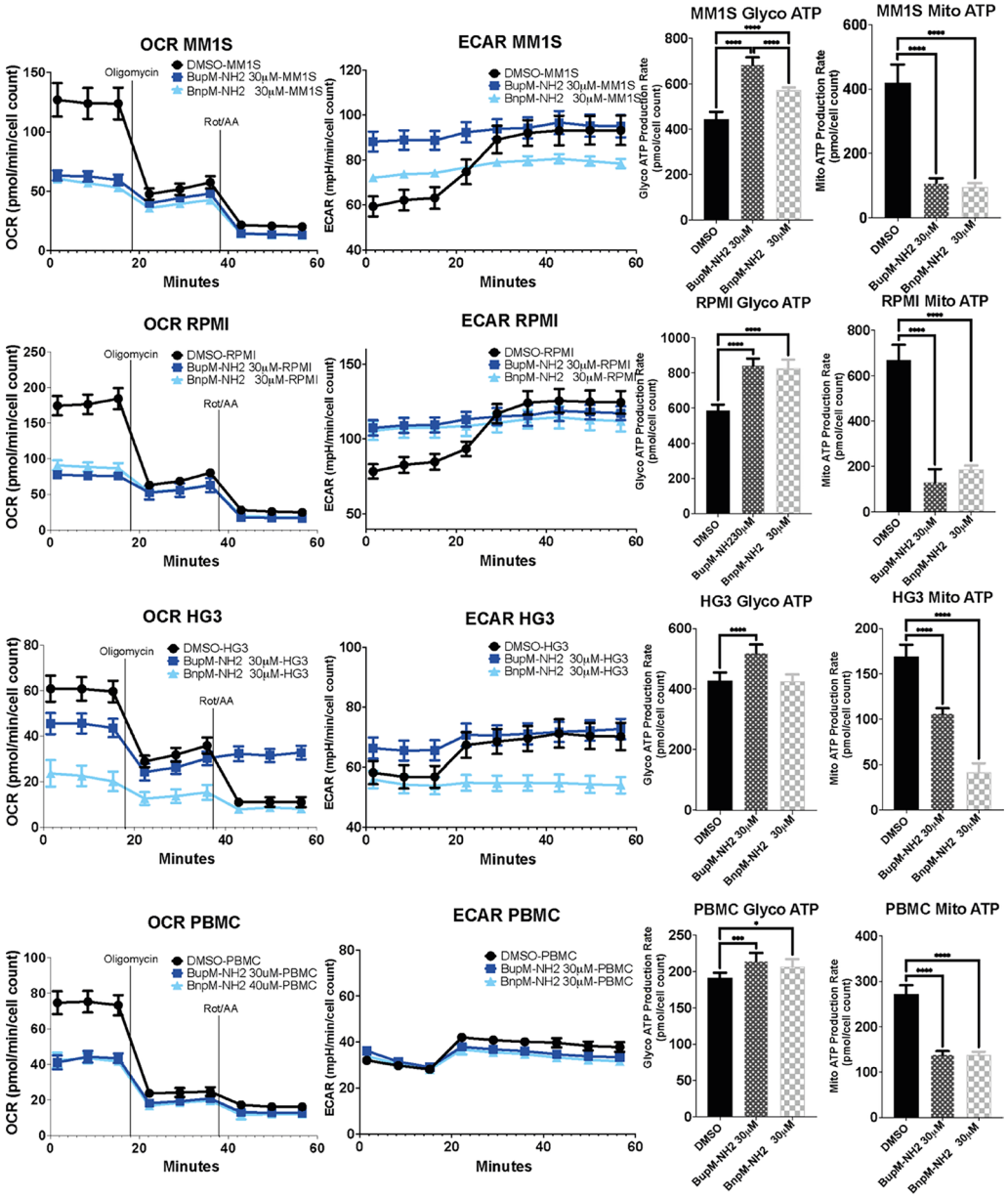

Fig. 5 BupM-NH2 and BnpM-NH2 inhibits mitochondrial respiration. Metabolic flux analysis, measuring OCR and ECAR to calculate ATP production from OXPHOS and glycolysis, was conducted using Seahorse XFe96 on MM1S, RPMI-8226, and HG3 cells treated with BupM-NH2 and BnpM-NH2 (30 μM) for 24 h. The graph shows three basal respiration/acidification points and changes after oligomycin and antimycin A (AA)/rotenone (Rot) addition. ATP production rates for MM and CLL cells in response to BupM-NH2 and BnpM-NH2 treatment (30 μM) are calculated using OCR and ECAR and plotted in bar graph. Each column represents mean ± SEM of three independent Seahorse experiments with four replicate wells per experiment for each cell line. P values were determined by one-way ANOVA with Tukey's post analysis. Differences were considered statistically significant when $P \leq 0.05$

insignificant decrease in MitoTracker MFI in all the three cell lines (Fig. 6B).

These findings suggest that inhibition of mitochondrial respiration and reduction in ETC complex II and IV protein expression, induced by BupM-NH2 and particularly BnpM-NH2, does not result in increased ROS production at the mitochondrial level. However, BnpM-NH2, which exhibits greater toxicity and causes more substantial mitochondrial respiration suppression, may induce an increase in mitochondrial biogenesis to compensate for the energy deficit, as evidenced by the increase in MitoTracker fluorescence, albeit not statistically significant.

Patient-derived MM cells exhibit sensitivity to BnpM-NH2

We subsequently evaluated the toxicity of the compounds on MM cells obtained from patients at disease onset (NDMM) and after acquiring resistance to bortezomib, lenalidomide and dexamethasone (RRMM)

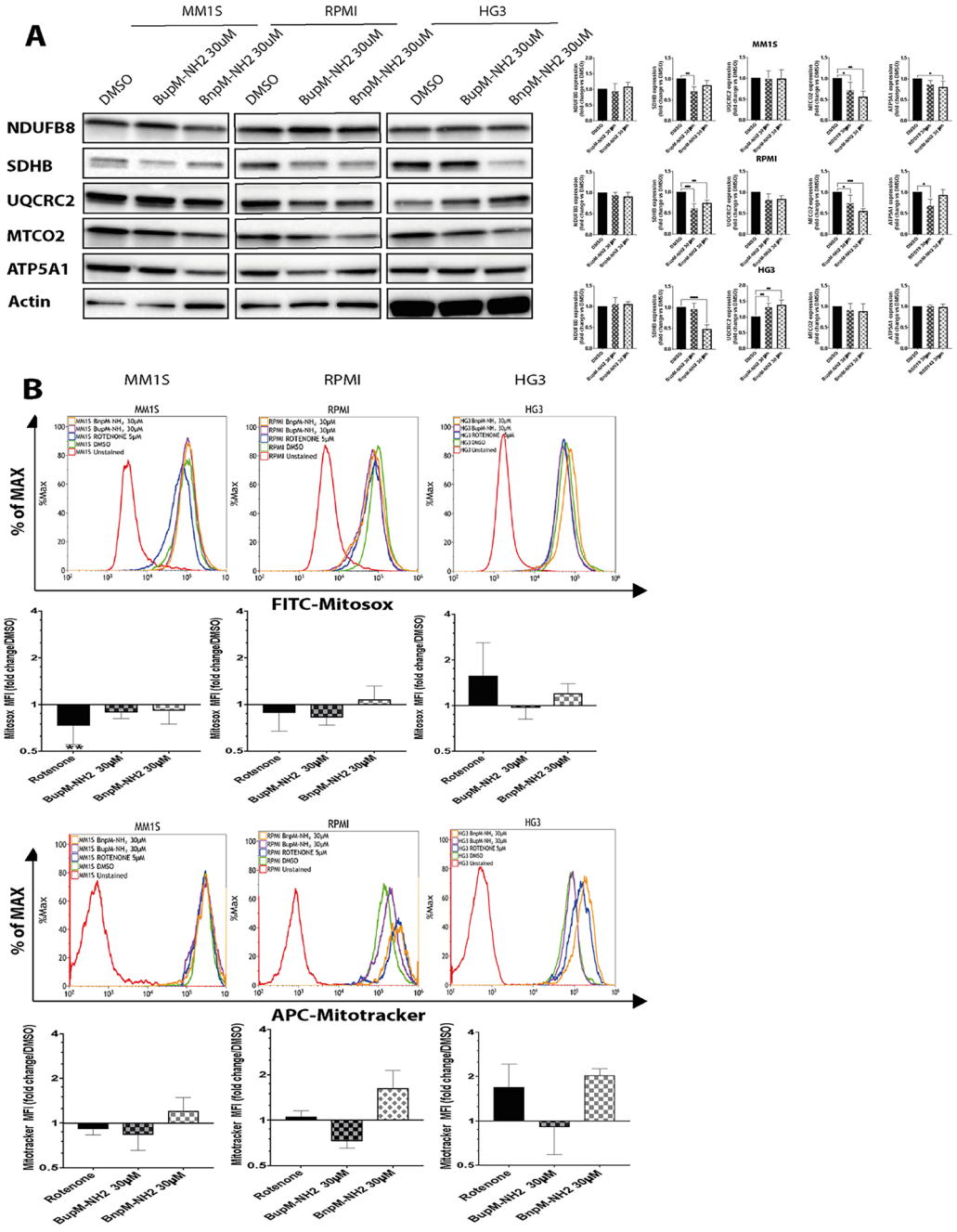

Fig. 6 The HIV protease inhibitors and BnpM-NH_2 affect the respiratory chain function altering the the expression of complex II and IV proteins. (**A**) WB analysis of NDUFB8, SDHB, UQCRC2, MTCO2, ATP5A1, and Actin expression in MM1S, RPMI-8226, and HG3 cells treated with BupM-NH2 and BnpM-NH2 (30 μM) for 48 h was performed. The intensity of NDUFB8, SDHB, UQCRC2, MTCO2, ATP5A1, and Actin intensity normalized to actin were quantified and plotted as bar graphs. The results are presented as mean ± SD of at least three replicates. (**B**) ROS production and mitochondrial mass in MM and CLL cells treated with BupM-NH_2 and BnpM-NH_2 (30 μM) for 24 h were assessed using mitosox and mitotracker assays. FACS analysis was employed to detect median fluorescent intensity (MFI), which was reported on a bar graph. Data, presented as mean ± SD, were obtained from at least three independent experiments. Significant differences ($P \leq 0.05$) were determined by one-way ANOVA with Tukey's post analysis

(Supplementary Fig. 5). Given limited yield of $CD138^+$ cells, a flow cytometry–based mitochondrial marker was prioritized to minimize input while enabling time-resolved analyses; MitoTracker Red CMXRos was therefore used as an initial proxy pending orthogonal validation. Because MitoTracker Red CMXRos is membrane potential–dependent, increased fluorescence can reflect changes in mitochondrial membrane potential (Δψm) as well as mitochondrial content; thus, increases

should be interpreted as indicative rather than definitive for mass expansion.

Group comparisons are based on a small ex vivo cohort (NDMM $n=3$; RRMM $n=5$) at a single dose and timepoint, without a priori power. Despite this limitation, BnpM-NH2 showed greater activity in NDMM at 30 µM and 48 h, whereas RRMM effects were modest and not statistically significant. Indeed, in NDMM, BnpM-NH2 reduced viability by 60% (D60.39 ± 12.55, $p<0.0001$) and increased apoptosis by 40% at 48 h (D-38.92 ± 12.55, $p=0.0092$) (Fig. 6A), consistent with MM OXPHOS reliance. In RRMM cells, cell viability decreased by approximately 15% (D16.42 ± 8.8, $p=0.121$), though not statistically significant, and was mainly linked to increased necrotic population (data not statistically significant) (Fig. 7A).

In our subsequent analysis, we evaluated the effects of two HIV protease inhibitors on mitochondrial function by quantifying ROS production using MitoSOX and mitochondrial mass using MitoTracker. In NDMM cells treated with BupM-NH2 and BnpM-NH2, ROS production increased at 6 and 24 h post-treatment, although the difference was not statistically significant (Fig. 7B). This oxidative stress was accompanied by increased MitoTracker Red signal (a Δψm-dependent proxy) in BnpM-NH2 treated cells (Δ1.24 ± 0.093, $p=0.088$), consistent with but not definitive for increased mitochondrial content (Fig. 7B).

In RRMM cells, BupM-NH2 and BnpM-NH2 significantly elevated ROS production at 3 h, showing an almost tenfold increase (Δ9.32 ± 0.97, $p=0.0047$; Δ8.09 ± 0.81, $p=0.041$), but did not significantly affect ROS production at 6 and 24 h post-treatment. Both treatments increased the mitochondrial mass, as shown by the MFI intensity (Δ0.57 ± 0.19, $p=0.042$; Δ0.38 ± 0.19, $p=0.16$) potentially due to stress in the respiratory chain function (Fig. 7B).

Thus, in a stromal-free ex vivo assay, NDMM $CD138^+$ cells showed greater sensitivity to BnpM-NH2 than RRMM; confirmation in microenvironment-inclusive systems is a next step.

The reduced cytotoxicity of BnpM-NH2 in drug-resistant MM cells may be attributed to elevated mitochondrial activity and enhanced anti-stress response, characteristics of resistant MM cells. The increase in ROS after 3 h of treatment with BupM-NH2 and BnpM-NH2 indicates these drugs impact mitochondrial function in RRMM cells, and their toxicity might be augmented when combined with therapies targeting the anti-stress response pathway. Preliminary data on the bortezomib-resistant MM cell line (OPM2-R) showed these HIV protease inhibitors increased cell death by approximately 10–15% more than bortezomib treatment. Furthermore, BnpM-NH2 significantly elevated ROS production at 24 h, which could be mitigated by the upregulated anti-stress response pathway in drug-resistant MM cells (Supplementary Fig. 6) [55].

Consequently, BnpM-NH2 has emerged as a promising novel treatment for MM, warranting investigation in preclinical studies. It holds substantial potential to enhance the efficacy of existing clinical therapies for MM through synergistic interactions.

Discussion

Our work reveals a contrasting mechanism in MM and CLL of BupM-NH2 and BnpM-NH2, previously studied in liver cancer where they induced autophagy. We showed that BupM-NH2 and BnpM-NH2 exert their anti-tumor effects by simultaneously disrupting two critical cellular processes: mitochondrial energy production and autophagy-mediated recycling. This dual-inhibition mechanism provides a multi-pronged attack on cancer cell survival, targeting specific mitochondrial respiratory chain complexes.

Mitochondrial metabolism is linked to MM progression and CLL transformation, providing greater resistance to cancer therapies by bolstering mechanisms targeted by first line cancer treatments. Studies have suggested that inhibiting mitochondrial respiration through complex I and II inhibitors or uncoupling agents could effectively treat hematologic disorders and sensitize drug-resistant tumors to therapy [15, 22].

In this study, we investigated and analyzed the antitumor properties of two precursors, BupM-NH2 and BnpM-NH2, of the HIV protease inhibitor darunavir analogs (44). Darunavir, the latest protease inhibitor (PI) to receive FDA approval, is recognized for its robust genetic barrier and its efficacy, particularly in combating multidrug-resistant strains of HIV. Several darunavir analogs with improved safety profiles and other pharmacological properties have been synthesized to develop more effective HIV treatments, specifically to overcome drug resistance. In this context, we synthesized BupM-NH2 and BnpM-NH2. Although Darunavir has been shown to have no antitumor effects, its simplified analogs have been shown to disrupt various oncogene-activated pathways (56) such as nelfinavir. Darunavir and nelfinavir share a hydroxyethyleneamine core but differ in their side substituents, as well as the internal pendants within the core. The two precursors of darunavir analogs have a free amino group in the hydroxyethyleneamine core that could be probably fundamental for antitumor properties as known for similar compounds [55]. Consequently, we evaluated whether BupM-NH2 and BnpM-NH2 exhibit antitumor properties. BupM-NH2 and BnpM-NH2 were found to be toxic mainly to MM and CLL cells but had a lesser impact on normal PBMC.

The mechanism of action of these compounds differed from previous findings in hepatocarcinoma cells.

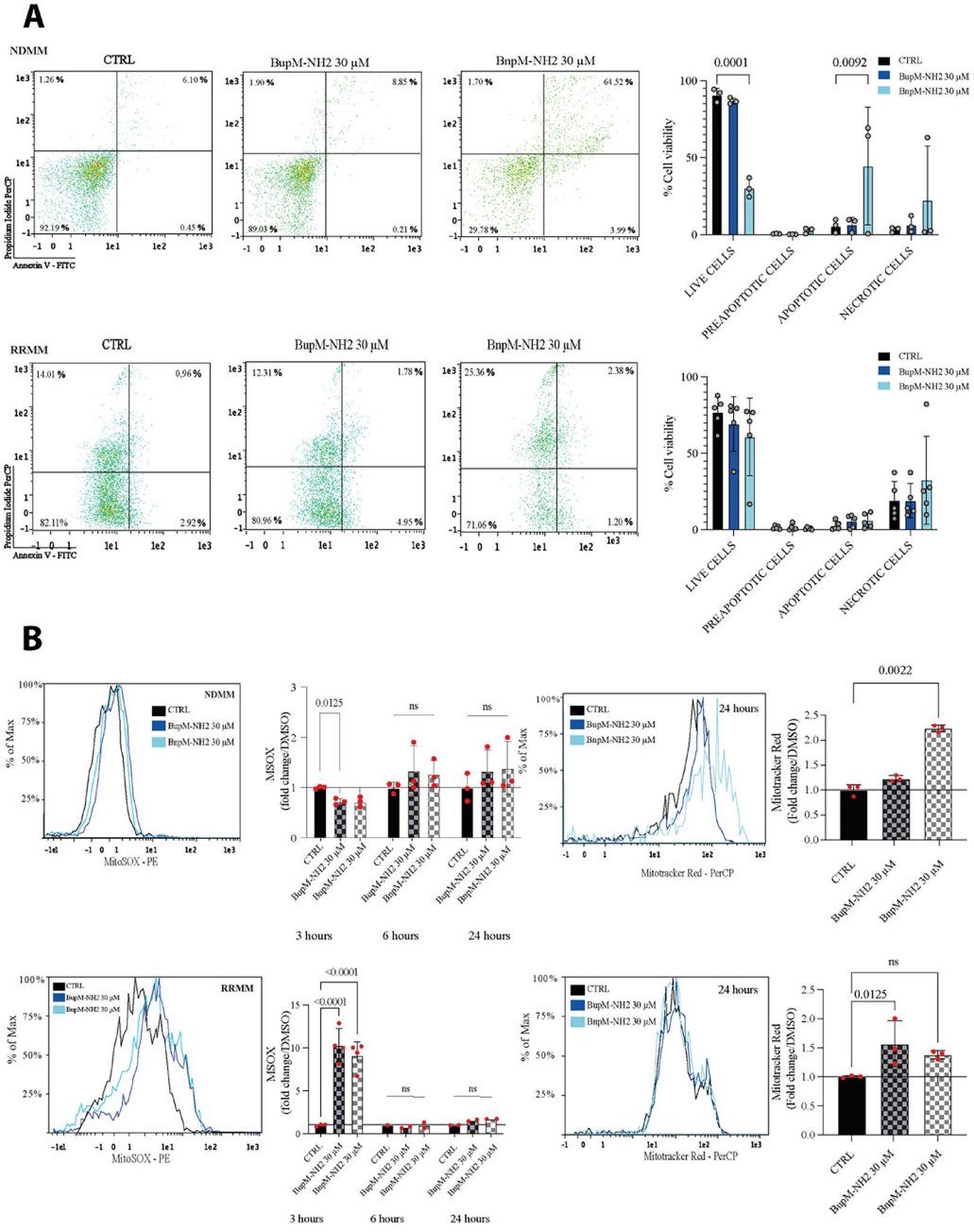

Fig. 7 Patient-derived MM cells exhibit sensitivity to BnpM-NH2 treatment. (**A**) Flow cytometric analysis of Annexin V/PI staining on MM samples from two patient cohorts: newly diagnosed multiple myeloma (NDMM) and relapsed/refractory multiple myeloma (RRMM). Apoptosis quantification was performed on pooled data from three NDMM and five RRMM patient samples, following treatment with BupM-NH2 and BnpM-NH2 (30µM) for 48 h. (**B**) Mitochondrial ROS (MitoSOX) and mitochondrial mass (MitoTracker) were measured in NDMM and RRMM cells at the indicated time points following treatment. Data are presented as mean ± SD from independent biological replicates ($n = 3$ NDMM, $n = 5$ RRMM), each analyzed in technical triplicate. Exact P-values are reported in the graphs; statistical significance was assessed using one-way ANOVA followed by Tukey's post-hoc test Statistical significance was considered at $P \leq 0.05$

BnpM-NH2 showed higher cytotoxicity against hematological malignancies than BupM-NH2, which was more effective against hepatocarcinoma. Their cytotoxicity occurred through respiratory chain inhibition, reducing complex IV protein expression in MM cells and complex II in CLL cells. BupM-NH2 and BnpM-NH2 induce an energetic deficit by disrupting mitochondrial respiration. While energy depletion typically triggers autophagy to generate metabolites through degradation of cellular components, autophagy inhibition by these compounds worsens the energetic deficit and impairs proteostasis. This severe energy shortage and reduced ATP supply may

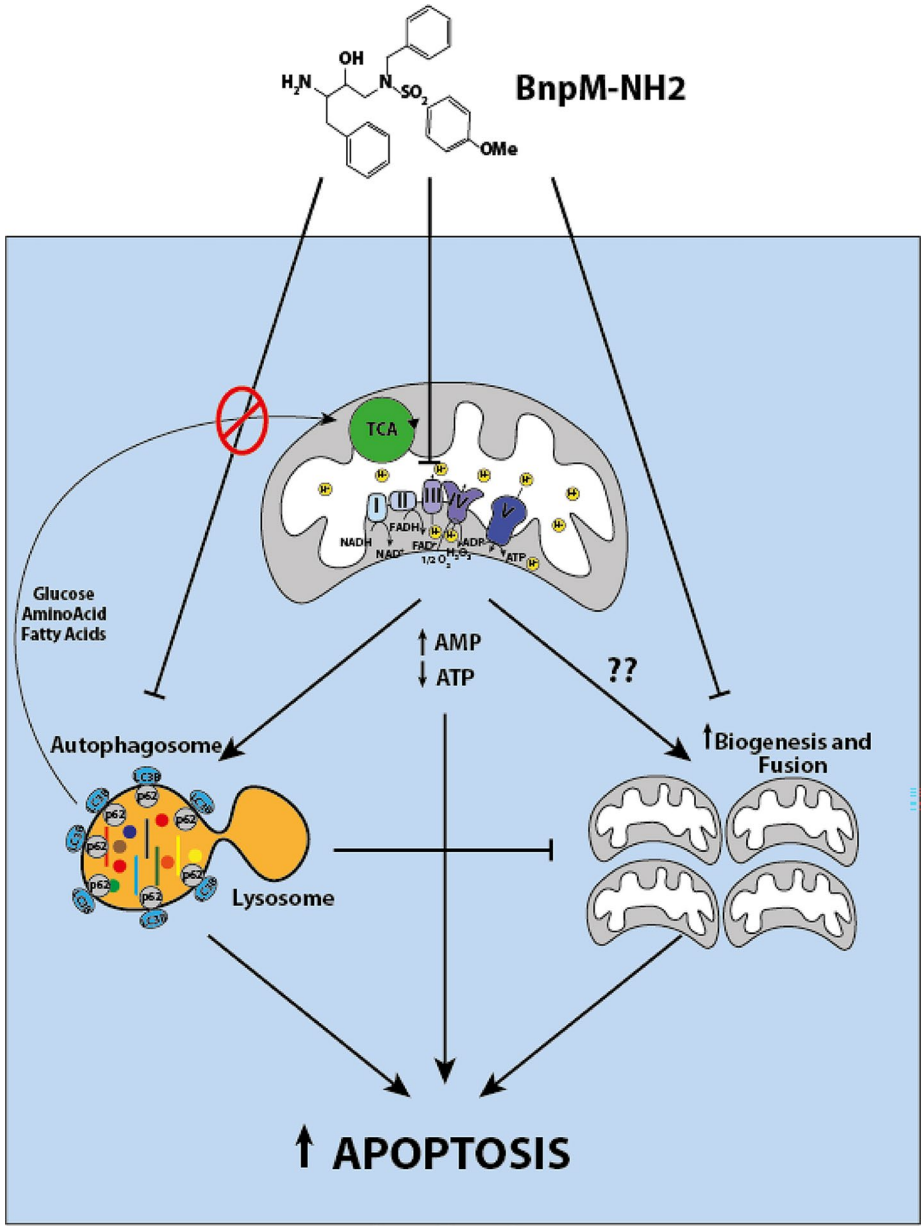

Fig. 8 Schematic representation of the mechanisms of BnpM-NH2 cytotoxicity on tumor cell. BnpM-NH2 inhibits mitochondrial respiration, thereby inducing energetic stress, which subsequently activates autophagy and could lead to mitochondrial biogenesis, as compensatory effect. Additionally, BnpM-NH2 inhibits autophagy, potentially by blocking autophagosome-lysosome fusion. The inhibition of autophagy exacerbates energetic stress, leading to apoptosis in tumor cells that are sensitive to therapy. Conversely, in therapy-resistant cells, a high mitochondrial mass can counteract the energetic stress induced by BnpM-NH2, thereby diminishing its cytotoxicity

impair ER stress response, leading to apoptosis via Caspase 3 activation (Fig. 8).

It is noteworthy that the toxicity of these two drugs is lower in normal PBMC cells than in tumor cells, which may make them a viable therapeutic option to be explored in future preclinical models. However, PBMCs, which comprise a heterogeneous mix of immune cells primarily enriched in T and B lymphocytes after Ficoll separation, are primary cells that may be more susceptible to the absence of environmental stimuli in vitro. This could affect their drug response, potentially leading to outcomes that differ from those in vivo. Nevertheless, the heterogeneity and naive state of PBMCs may render them more vulnerable to cell death than stable cell lines, which are selected for survival and proliferation capabilities following genetic modifications that confer increased resistance to apoptosis.

Analyses of patient-derived MM cells have demonstrated that BnpM-NH2 significantly diminishes the viability of therapy-sensitive MM (NDMM) by inducing

apoptosis. Concurrently, it exhibited some, albeit limited and not statistically significant, efficacy in reducing the viability of bortezomib-lenalidomide-dexamethasone-resistant MM cells (RRMM). The diminished effectiveness of BnpM-NH2 in resistant MM may be attributed to the elevated mitochondrial mass, characterized by elevated ubiquinone complex I levels, which enables these cells to counteract or neutralize the impact of mitochondrial respiration inhibition. This, in turn, prevents the energetic stress that typically induces apoptosis. Anyway, further validation with a larger sample of MM cells from patients who developed resistance is needed.

However it is noteworthy that preliminary data indicate that these protease inhibitors disrupt mitochondrial function and elevate ROS production of in bortezomib-resistant multiple myeloma (MM) cell lines (OOPM2-R), despite exhibiting low toxicity. This increase in ROS levels and related damage could be counteracted by enhanced anti-stress mechanisms in therapy-resistant MM cells. These observations are encouraging because they imply that BupM-NH2 and BnpM-NH2 could potentially function alongside existing first-line treatments or new investigational drugs targeting altered cellular pathways in resistant MM cells.

Cancer cells, such as MM and leukemia cells, can acquire drugs resistance by enhancing mitochondrial metabolism through modifications to their internal metabolism, or by exchanging mitochondria [56, 57]. Consequently, inhibiting the mitochondrial respiration of tumor cells with specific agents has been demonstrated to re-sensitize them to antitumor therapies.

In this regard, BupM-NH2 and BnpM-NH2 may prove to be viable therapeutic options for the treatment of primary blood cancers and relapses, as well as for use in combination with existing therapies in clinical practice. A key contribution of our work is the demonstration that BnpM-NH2 is effective against multiple myeloma cells taken directly from patients, including those resistant to standard therapies like bortezomib. This suggests a potential clinical application for overcoming drug resistance, a major challenge in treating multiple myeloma. The general strategy of repurposing HIV protease inhibitors for cancer treatment is not new. Other inhibitors, such as nelfinavir and ritonavir, have been extensively studied for their anti-tumor properties in various cancers, including multiple myeloma. Inhibition of complex I and II activity has been found to increase the sensitivity of MM cells to venetoclax [22], an inhibitor of the anti-apoptotic protein BCL2, and to re-sensitize CLL cells that are resistant to venetoclax [58].

Given the pivotal role of mitochondria in carcinogenesis and drug resistance, various therapeutic strategies have been devised to target their function. These strategies primarily aim to inhibit OXPHOS, mitochondrial metabolism, mitochondrial fission, and apoptosis-related signaling pathways in cancer cells. Molecules that inhibit ETC complexes I (e.g., metformin, MS-L6, and IACS-010759), II (e.g., lonidamine), III (e.g., Antimycin A, ME-344), and V (e.g., Bafilomycin A1) have demonstrated efficacy in preclinical studies [59]. However, clinical investigations have identified dose-limiting toxicities, such as metabolic acidosis and neurotoxicity, resulting in the discontinuation of numerous trials due to narrow therapeutic windows [60]. Another approach involves molecules such as CPI-163, which target Krebs cycle enzyme complexes such as pyruvate dehydrogenase (PDH) and alpha-ketoglutarate dehydrogenase (KGDH) [61], or compounds such as 968 and CB-839, which inhibit enzymes such as glutaminase that provide acetyl-CoA to the Krebs cycle from glutamine degradation [62]. Inhibiting these pathways reduces the levels of metabolic intermediates essential for epigenetic modifications and macromolecule synthesis necessary for tumor growth, while also decreasing NADH and FADH2 production, thereby affecting ETC activity and ATP production. ETC inhibitors also decelerate the Krebs cycle and metabolite synthesis. To date, clinical trials evaluating metformin and CPI-163 have yielded controversial results. While metformin has exhibited promising preclinical outcomes, clinical trials have produced mixed data, with some studies reporting efficacy in various tumors, whereas others have shown no significant antitumor effects [63–66]. CPI-613 has demonstrated a significant therapeutic index with promising Phase I and II results in pancreatic cancer and acute myeloid leukemia (NCT01835041) [67, 68]. However, CPI-613 Phase III clinical trials for relapsed/refractory acute myeloid leukemia or metastatic pancreatic adenocarcinoma (NCT03504410 and NCT03504423) did not demonstrate any benefit in overall survival.

In comparison to metformin and CPI-613, BupM-NH2 and BnpM-NH2 exhibited a different mechanism, primarily acting on complexes II and IV and influencing autophagy [69, 70]. Therefore, it is essential to assess the antitumor efficacy of these compounds in vivo and to determine their toxicities. Indeed, the study's limitations, inherent in its exclusive in vitro design, stem from its inability to replicate the intricate dynamics of a living organism, including metabolic processes, immune responses, and the interplay between various organ systems. This limitation prevents accurate evaluation of the effects of drugs on the microenvironment, stromal cells, and immune system cells, as well as their potential non-specific toxicity and side effects, which may impede their practical application. Additionally, the in vitro model does not allow for the evaluation of drug absorption, distribution, metabolism, and excretion, which could result in discrepancies between in vitro and in vivo findings.

Future in vivo studies will be crucial to clarify the effects of the two drugs on the immune system and stromal cells, particularly regarding the activation and exhaustion of CD8 cytotoxic T lymphocytes, as well as the immunosuppressive functions of regulatory T cells (Treg) and myeloid-derived suppressor cells (MDSC), and the protumor function of stromal cells. Additionally, given the inhibitory activity of these compounds on the respiratory chain, it would be beneficial to determine their cardio- and neurotoxicity-related side effects of these compounds in preclinical models. An additional potential limitation is the necessity for higher concentrations of the compounds BupM-NH2 and BnpM-NH2 to achieve antitumor efficacy in vitro, in comparison to other protease inhibitors such as nelfinavir, which have exhibited antitumor properties at low concentrations, comparable to those present in human plasma (3–7 μM).

Nevertheless, it is conceivable that BupM-NH2 and BnpM-NH2 possess superior bioavailability and tolerability in vivo, which may render them more effective at higher concentrations than those of other protease inhibitors. Therefore, determining the maximum tolerated dose, side effects, and bioavailability of these compounds in animal models will be essential to establish whether the concentrations of BupM-NH2 and BnpM-NH2, tested in vitro as antitumor agents, are achievable and tolerable. In humans, when darunavir is administered orally in conjunction with ritonavir at daily dosages of 800 mg and 100 mg, respectively, it achieves an average maximum plasma concentration (Cmax) of 15 μM within 2–3 h, with some individuals experiencing peaks nearing 20 μM [71]. Consequently, if BupM-NH2 and BnpM-NH2 exhibit pharmacokinetics and pharmacodynamics analogous to those of darunavir, they would attain concentrations below 30 μM, a level demonstrated to exert cytotoxic effects on tumor cells. However, the current inability to predict the in vivo metabolism of these two compounds poses challenges to understanding how biotransformation might influence their bioavailability, activity, and overall pharmacokinetic and pharmacodynamic profiles.

In summary, the two compounds exhibited promising antitumor efficacy in blood cancers by modulating distinct mechanisms compared with other HIV protease inhibitors. Therefore, it is crucial to conduct further preclinical research on the impact of altering these mechanisms mediated by BupM-NH2 and BnpM-NH2 on tumor progression and the development of resistance to anticancer treatments while simultaneously assessing potential cardiac and neurological toxicity.

Abbreviations

AKT	Protein kinase B
ATF4	Activating transcription factor 4
BECN1	Beclin1
CLL	Chronic lymphatic leukemia
Δψm	Mitochondrial membrane potential
ECAR	Extracellular acidification rate
eIF2α	Eukaryotic translation initiation factor 2 alpha
ER	Endoplasmic reticulum
ERK	Extracellular regulated kinase
ETC	Electron transport chain
HIV	Human immunodeficiency virus
IC_{50}	Half-maximal inhibitory concentration
KGDH	Alpha-ketoglutarate dehydrogenase
MDSC	Myeloid-derived suppressor cells
MM	Multiple myeloma
MTCO2	Mitochondrially encoded cytochrome C oxidase II
OCR	Oxygen Consumption Rate
OXPHOS	Oxidative Phosphorylation
PBMC	Peripheral Blood Mononuclear Cells
PDH	Pyruvate dehydrogenase
PI	Propidium Iodide
ROS	Reactive Oxygen Species
SRC	Spare Respiratory Capacity
STAT3	Signal Transducer and Activator of Transcription 3
SDHB	Succinate Dehydrogenase Complex Iron Sulfur Subunit B
TCA	Tricarboxylic Acid Cycle
Treg	regulatory T cells
UPR	Unfolded Protein Response
XBP1s	Spliced form of X-box Binding Protein 1

Supplementary Information

The online version contains supplementary material available at https://doi.org/10.1186/s12935-025-04142-w.

Supplementary Material 1.

Supplementary Material 2.

Acknowledgements
Not applicable.

Author contributions
M.M., M.S., E.L.S., M.G., E.G., S.P. performed all the in vitro experiment. L.V. and T.S. carried out FACS analysis. A.S. synthesized the two drugs. M.F., M.F.A., L.C., P.L., A.R. and A.G. provide expertise and feedback. S.C. conceived and designed the study and drafted the manuscript. All authors discussed the results and contributed to the final manuscript.

Funding
This work was supported by Italian Ministry of Health (Ricerca Corrente).

Data availability
No datasets were generated or analysed during the current study.

Declarations

Ethics approval and consent to participate
All human samples used in this study were obtained with the approval of the Ethics Committee of Policlinico Catania 1, (ID: n.34/2019/PO).

Consent for publication
The patients/participants provided their written informed consent to participate in this study.

Competing interests
The authors declare no competing interests.

Author details
[1]Laboratory of Preclinical and Translational Research, Centro di Riferimento Oncologico della Basilicata (IRCCS-CROB), Rionero in Vulture (PZ) 85028, Italy

[2]Department of Biomedical and Biotechnological Sciences, Division of Medical Biochemistry, University of Catania, Catania 95123, Italy
[3]Department of Basic and Applied Sciences, University of Basilicata, Viale dell'Ateneo Lucano 10, Potenza 85100, Italy
[4]Department of Health Sciences, University of Basilicata, Viale dell'Ateneo Lucano 10, Potenza 85100, Italy
[5]Department of Chemistry, University of Rome La Sapienza, p.le Aldo Moro 5, Roma 00185, Italy
[6]Department of General Surgery and Medical-Surgical Specialties, Hematology Section, University of Catania, Catania 95123, Italy
[7]Department of Medical Biotechnologies, University of Siena, Siena 53100, Italy
[8]Sbarro Institute for Cancer Research and Molecular Medicine, Center for Biotechnology, Department of Biology, College of Science and Technology, Temple University, Philadelphia, PA 19122, USA
[9]Laboratory of Molecular Oncology, Responsible Research Hospital, Campobasso 86100, Italy
[10]Clinical and Translational Oncology, Scuola Superiore Meridionale (SSM), Napoli 80138, Italy
[11]S.H.R.O. Italia Foundation ETS, Candiolo 10060, TO, Italy

Received: 6 June 2025 / Accepted: 16 December 2025
Published online: 23 December 2025

References

1. Mecca M, Picerno S, Cortellino S. The killer's web: interconnection between inflammation, epigenetics and nutrition in cancer. Int J Mol Sci. 2024;25:2750.
2. Cortellino S, Longo VD. Metabolites and immune response in tumor microenvironments. Cancers. 2023;15:3898.
3. Koppenol WH, Bounds PL, Dang CV. Otto warburg's contributions to current concepts of cancer metabolism. Nat Rev Cancer. 2011;11:325–37.
4. Hanahan D, Monje M. Cancer hallmarks intersect with neuroscience in the tumor microenvironment. Cancer Cell. 2023;41:573–80.
5. Yuneva MO, Fan TWM, Allen TD, Higashi RM, Ferraris DV, Tsukamoto T, et al. The metabolic profile of tumors depends on both the responsible genetic lesion and tissue type. Cell Metab. 2012;15:157–70.
6. Mayers JR, Torrence ME, Danai LV, Papagiannakopoulos T, Davidson SM, Bauer MR, et al. Tissue of origin dictates branched-chain amino acid metabolism in mutant *Kras* -driven cancers. Science. 2016;353:1161–5.
7. Cortellino S, D'Angelo M, Quintiliani M, Giordano A. Cancer knocks you out by fasting: cachexia as a consequence of metabolic alterations in cancer. J Cell Physiol. 2025;240:e31417.
8. Marlein CR, Piddock RE, Mistry JJ, Zaitseva L, Hellmich C, Horton RH, et al. CD38-Driven Mitochondrial Trafficking Promotes Bioenergetic Plasticity in Multiple Myeloma. Cancer Res. 2019;79:2285–97.
9. Liu H, He J, Koh SP, Zhong Y, Liu Z, Wang Z, et al. Reprogrammed marrow adipocytes contribute to myeloma-induced bone disease. Sci Transl Med. 2019;11:eaau9087.
10. Jitschin R, Hofmann AD, Bruns H, Gießl A, Bricks J, Berger J, et al. Mitochondrial metabolism contributes to oxidative stress and reveals therapeutic targets in chronic lymphocytic leukemia. Blood. 2014;123:2663–72.
11. Pan B, Xu Z, Du K, Gao R, Zhang J, Yin H, et al. Investigation of fatty acid metabolism in chronic lymphocytic leukemia to guide clinical outcome and therapy. Ann Hematol. 2024;103:1241–54.
12. Weisel FJ, Mullett SJ, Elsner RA, Menk AV, Trivedi N, Luo W, et al. Germinal center B cells selectively oxidize fatty acids for energy while conducting minimal glycolysis. Nat Immunol. 2020;21:331–42.
13. Gonsalves WI, Jang JS, Jessen E, Hitosugi T, Evans LA, Jevremovic D, et al. In vivo assessment of glutamine anaplerosis into the TCA cycle in human premalignant and malignant clonal plasma cells. Cancer Metab. 2020;8:29.
14. Liu PP, Liu J, Jiang WQ, Carew JS, Ogasawara MA, Pelicano H, et al. Elimination of chronic lymphocytic leukemia cells in stromal microenvironment by targeting CPT with an antiangina drug perhexiline. Oncogene. 2016;35:5663–73.
15. Barbato A, Scandura G, Puglisi F, Cambria D, La Spina E, Palumbo GA, et al. Mitochondrial bioenergetics at the onset of drug resistance in hematological malignancies: an overview. Front Oncol. 2020;10:604143.
16. Keoh LQ, Chiu CF, Ramasamy TS. Metabolic plasticity and cancer stem cell metabolism: exploring the glycolysis-OXPHOS switch as a mechanism for resistance and tumorigenesis. Stem Cell Rev Rep. 2025;21:2446–68.
17. Nie Y, Yun X, Zhang Y, Wang X. Targeting metabolic reprogramming in chronic lymphocytic leukemia. Exp Hematol Oncol. 2022;11:39.
18. Nikesitch N, Lee JM, Ling S, Roberts TL. Endoplasmic reticulum stress in the development of multiple myeloma and drug resistance. Clinical & Translational Immunology. 2018;7:e1007.
19. Khateb A, Ronai ZA. Unfolded protein response in leukemia: from basic understanding to therapeutic opportunities. Trends Cancer. 2020;6:960–73.
20. Boise LH, Kaufman JL, Bahlis NJ, Lonial S, Lee KP. The tao of myeloma. Blood. 2014;124:1873–9.
21. Rossi D, Spina V, Gaidano G. Biology and treatment of Richter syndrome. Blood. 2018;131:2761–72.
22. Bajpai R, Sharma A, Achreja A, Edgar CL, Wei C, Siddiqa AA, et al. Electron transport chain activity is a predictor and target for venetoclax sensitivity in multiple myeloma. Nat Commun. 2020;11:1228.
23. Besse L, Besse A, Mendez-Lopez M, Vasickova K, Sedlackova M, Vanhara P, et al. A metabolic switch in proteasome inhibitor-resistant multiple myeloma ensures higher mitochondrial metabolism, protein folding and sphingomyelin synthesis. Haematologica. 2019;104:e415–9.
24. Zaal EA, De Grooth HJ, Oudaert I, Langerhorst P, Levantovsky S, Van Slobbe GJJ, et al. Targeting coenzyme Q10 synthesis overcomes bortezomib resistance in multiple myeloma. Mol Omics. 2022;18:19–30.
25. Chen Z, Simon-Molas H, Cretenet G, Valle-Argos B, Smith LD, Forconi F, et al. Characterization of metabolic alterations of chronic lymphocytic leukemia in the lymph node microenvironment. Blood. 2022;140:630–43.
26. Burger KL, Fernandez MR, Meads MB, Sudalagunta P, Oliveira PS, Renatino Canevarolo R, et al. CK1δ and CK1ε signaling sustains mitochondrial metabolism and cell survival in multiple myeloma. Cancer Res. 2023;83:3901–19.
27. Waldschmidt JM, Kloeber JA, Anand P, Frede J, Kokkalis A, Dimitrova V, et al. Single-Cell profiling reveals metabolic reprogramming as a resistance mechanism in *BRAF* -Mutated multiple myeloma. Clin Cancer Res. 2021;27:6432–44.
28. Joshua DE, Bryant C, Dix C, Gibson J, Ho J. Biology and therapy of multiple myeloma. Med J Aust. 2019;210:375–80.
29. Cilta-cel. OK'd for multiple myeloma. Cancer Discov. 2022;12:1176–1176.
30. Stilgenbauer S. Prognostic markers and standard management of chronic lymphocytic leukemia. Hematology. 2015;2015:368–77.
31. Yang Y, Ikezoe T, Nishioka C, Bandobashi K, Takeuchi T, Adachi Y, et al. NFV, an HIV-1 protease inhibitor, induces growth arrest, reduced Akt signalling, apoptosis and docetaxel sensitisation in NSCLC cell lines. Br J Cancer. 2006;95:1653–62.
32. Srirangam A, Mitra R, Wang M, Gorski JC, Badve S, Baldridge L, et al. Effects of HIV protease inhibitor Ritonavir on Akt-Regulated cell proliferation in breast cancer. Clin Cancer Res. 2006;12:1883–96.
33. Pajonk F, Himmelsbach J, Riess K, Sommer A, McBride WH. The human immunodeficiency virus (HIV)-1 protease inhibitor saquinavir inhibits proteasome function and causes apoptosis and radiosensitization in non-HIV-associated human cancer cells. Cancer Res. 2002;62:5230–5.
34. Ikezoe T, Saito T, Bandobashi K, Yang Y, Koeffler HP, Taguchi H. HIV-1 protease inhibitor induces growth arrest and apoptosis of human multiple myeloma cells via inactivation of signal transducer and activator of transcription 3 and extracellular signal-regulated kinase 1/2. Mol Cancer Ther. 2004;3:473–9.
35. Jiang W, Mikochik PJ, Ra JH, Lei H, Flaherty KT, Winkler JD, et al. HIV protease inhibitor nelfinavir inhibits growth of human melanoma cells by induction of cell cycle arrest. Cancer Res. 2007;67:1221–7.
36. Kumar S, Bryant CS, Chamala S, Qazi A, Seward S, Pal J, et al. Ritonavir blocks AKT signaling, activates apoptosis and inhibits migration and invasion in ovarian cancer cells. Mol Cancer. 2009;8:26.
37. Yang Y, Ikezoe T, Takeuchi T, Adachi Y, Ohtsuki Y, Takeuchi S, et al. HIV-1 protease inhibitor induces growth arrest and apoptosis of human prostate cancer LNCaP cells *in vitro* and *in vivo* in conjunction with blockade of androgen receptor STAT3 and AKT signaling. Cancer Sci. 2005;96:425–33.
38. Gupta AK, Cerniglia GJ, Mick R, McKenna WG, Muschel RJ. HIV protease inhibitors block Akt signaling and radiosensitize tumor cells both *In vitro* and *In vivo*. Cancer Res. 2005;65:8256–65.
39. Buijsen J, Lammering G, Jansen RLH, Beets GL, Wals J, Sosef M, et al. Phase I trial of the combination of the Akt inhibitor nelfinavir and chemoradiation for locally advanced rectal cancer. Radiother Oncol. 2013;107:184–8.
40. Driessen C, Kraus M, Joerger M, Rosing H, Bader J, Hitz F, et al. Treatment with the HIV protease inhibitor nelfinavir triggers the unfolded protein response and may overcome proteasome inhibitor resistance of multiple myeloma in combination with bortezomib: a phase I trial (SAKK 65/08). Haematologica. 2016;101:346–55.

41. Gills JJ, LoPiccolo J, Tsurutani J, Shoemaker RH, Best CJM, Abu-Asab MS, et al. Nelfinavir, A lead HIV protease inhibitor, is a Broad-Spectrum, anticancer agent that induces Endoplasmic reticulum Stress, Autophagy, and apoptosis *In vitro* and *In vivo*. Clin Cancer Res. 2007;13:5183–94.
42. Monini P, Sgadari C, Toschi E, Barillari G, Ensoli B. Antitumour effects of antiretroviral therapy. Nat Rev Cancer. 2004;4:861–75.
43. Sgadari C, Barillari G, Toschi E, Carlei D, Bacigalupo I, Baccarini S, et al. HIV protease inhibitors are potent anti-angiogenic molecules and promote regression of Kaposi sarcoma. Nat Med. 2002;8:225–32.
44. Driessen C, Müller R, Novak U, Cantoni N, Betticher D, Mach N, et al. Promising activity of nelfinavir-bortezomib-dexamethasone in proteasome inhibitor–refractory multiple myeloma. Blood. 2018;132:2097–100.
45. Mendez-Lopez M, Sutter T, Driessen C, Besse L. HIV protease inhibitors for the treatment of multiple myeloma. Clin Adv Hematol Oncol. 2019;17:615–23.
46. Rinaldi R, Miglionico R, Nigro I, D'Orsi R, Chiummiento L, Funicello M, et al. Two novel precursors of the HIV-1 protease inhibitor Darunavir target the UPR/Proteasome system in human hepatocellular carcinoma cell line HepG2. Cells. 2021;10:3052.
47. Tramutola F, Armentano MF, Berti F, Chiummiento L, Lupattelli P, D'Orsi R, et al. New heteroaryl carbamates: synthesis and biological screening in vitro and in mammalian cells of wild-type and mutant HIV-protease inhibitors. Bioorg Med Chem. 2019;27:1863–70.
48. Methods to Monitor ROS Production by Fluorescence Microscopy and Fluorometry [Internet]. In: Methods in Enzymology. Elsevier. 2014 [cited 2025 Oct 30]. page 243–62.Available from: https://linkinghub.elsevier.com/retrieve/pii/B9780124166189000133
49. Yang Y, Zhang G, Yang T, Gan J, Xu L, Yang H. A flow-cytometry-based protocol for detection of mitochondrial ROS production under hypoxia. STAR Protoc. 2021;2:100466.
50. Pyrko P, Kardosh A, Wang W, Xiong W, Schönthal AH, Chen TC. HIV-1 protease inhibitors nelfinavir and Atazanavir induce malignant glioma death by triggering Endoplasmic reticulum stress. Cancer Res. 2007;67:10920–8.
51. Besse A, Sedlarikova L, Buechler L, Kraus M, Yang CH, Strakova N, et al. HIV-protease inhibitors potentiate the activity of Carfilzomib in triple-negative breast cancer. Br J Cancer. 2024;131:918–30.
52. Wu Y, Chen Y, Yan X, Dai X, Liao Y, Yuan J, et al. Lopinavir enhances Anoikis by remodeling autophagy in a circRNA-dependent manner. Autophagy. 2024;20:1651–72.
53. Bono C, Karlin L, Harel S, Mouly E, Labaume S, Galicier L, et al. The human immunodeficiency virus-1 protease inhibitor nelfinavir impairs proteasome activity and inhibits the proliferation of multiple myeloma cells in vitro and in vivo. Haematologica. 2012;97:1101–9.
54. Xiang T, Du L, Pham P, Zhu B, Jiang S. Nelfinavir, an HIV protease inhibitor, induces apoptosis and cell cycle arrest in human cervical cancer cells via the ROS-dependent mitochondrial pathway. Cancer Lett. 2015;364:79–88.
55. Facchinetti V, Moreth M, Gomes CRB, Do Ó, Pessoa C, Rodrigues FAR, Cavalcanti BC, et al. Evaluation of (2S,3R)-2-(amino)-[4-(N-benzylarenesulfonamido)-3-hydroxy-1-phenylbutane derivatives: a promising class of anticancer agents. Med Chem Res. 2015;24:533–42.
56. Xia J, Zhang J, Wu X, Du W, Zhu Y, Liu X, et al. Blocking Glycine utilization inhibits multiple myeloma progression by disrupting glutathione balance. Nat Commun. 2022;13:4007.
57. Diehl FF, Lewis CA, Fiske BP, Vander Heiden MG. Cellular redox state constrains Serine synthesis and nucleotide production to impact cell proliferation. Nat Metab. 2019;1:861–7.
58. Playa-Albinyana H, Arenas F, Royo R, Giró A, López-Oreja I, Aymerich M, et al. Chronic lymphocytic leukemia patient-derived xenografts recapitulate clonal evolution to Richter transformation. Leukemia. 2024;38:557–69.
59. Du H, Xu T, Yu S, Wu S, Zhang J. Mitochondrial metabolism and cancer therapeutic innovation. Signal Transduct Target Ther. 2025;10:245.
60. Yap TA, Daver N, Mahendra M, Zhang J, Kamiya-Matsuoka C, Meric-Bernstam F, et al. Complex I inhibitor of oxidative phosphorylation in advanced solid tumors and acute myeloid leukemia: phase I trials. Nat. Med. 2023;29:115–26.
61. Stuart SD, Schauble A, Gupta S, Kennedy AD, Keppler BR, Bingham PM, et al. A strategically designed small molecule attacks alpha-ketoglutarate dehydrogenase in tumor cells through a redox process. Cancer Metab. 2014;2:4.
62. Li Y, Li B, Xu Y, Qian L, Xu T, Meng G, et al. GOT2 silencing promotes reprogramming of glutamine metabolism and sensitizes hepatocellular carcinoma to glutaminase inhibitors. Cancer Res. 2022;82:3223–35.
63. investigators MYME, Nanni O, Amadori D, De Censi A, Rocca A, Freschi A, et al. Metformin plus chemotherapy versus chemotherapy alone in the first-line treatment of HER2-negative metastatic breast cancer. The MYME randomized, phase 2 clinical trial. Breast Cancer Res Treat. 2019;174:433–42.
64. Goodwin PJ, Chen BE, Gelmon KA, Whelan TJ, Ennis M, Lemieux J, et al. Effect of Metformin vs placebo on invasive disease–free survival in patients with breast cancer: the MA.32 randomized clinical trial. JAMA. 2022;327:1963.
65. Arrieta O, Barrón F, Padilla MÁS, Avilés-Salas A, Ramírez-Tirado LA, Arguelles Jiménez MJ, et al. Effect of Metformin plus tyrosine kinase inhibitors compared with tyrosine kinase inhibitors alone in patients with epidermal growth factor Receptor–Mutated lung adenocarcinoma: a phase 2 randomized clinical trial. JAMA Oncol. 2019;5:e192553.
66. Brown JR, Chan DK, Shank JJ, Griffith KA, Fan H, Szulawski R et al. Phase II clinical trial of metformin as a cancer stem cell-targeting agent in ovarian cancer. JCI Insight [Internet] 2020 [cited 2025 Nov 6];Available from: http://insight.jci.org/articles/view/133247
67. Alistar AT, Desnoyers R, D'Agostino RJ, Pasche B. CPI-613 enhances FOLFIRINOX response rate in stage IV pancreatic cancer. Ann Oncol. 2016;27:vi228.
68. Pardee TS, Lee K, Luddy J, Maturo C, Rodriguez R, Isom S, et al. A phase I study of the First-in-Class antimitochondrial metabolism Agent, CPI-613, in patients with advanced hematologic Malignancies. Clin. Cancer Res. 2014;20:5255–64.
69. Pardee TS, Powell BL, Larson RA, Maly J, Keng M, Foster M, et al. Devimistat plus chemotherapy vs chemotherapy alone for older relapsed or refractory patients with AML: results of the ARMADA trial. Blood Neoplasia. 2024;1:100009.
70. Philip PA, Sahai V, Bahary N, Mahipal A, Kasi A, Rocha Lima CMS, et al. Devimistat (CPI-613) with modified Fluorouarcil, Oxaliplatin, Irinotecan, and leucovorin (FFX) versus FFX for patients with metastatic adenocarcinoma of the pancreas: the phase III AVENGER 500 study. J Clin Oncol. 2024;42:3692–701.
71. Jackson A, Else L, Higgs C, Karolia Z, Khoo S, Back D, et al. Pharmacokinetics and pharmacodynamics of the nucleoside sparing dual regimen containing rilpivirine plus darunavir/ritonavir in treatment-naïve HIV-1-infected individuals. HIV Clin Trials. 2018;19:31–7.

Publisher's note

Springer Nature remains neutral with regard to jurisdictional claims in published maps and institutional affiliations.